On the Performance Gain of Harnessing Non-Line-of-Sight Propagation for Visible Light-Based Positioning

Bingpeng Zhou, *Member, IEEE*, Yuan Zhuang, *Member, IEEE*, and Yue Cao, *Member, IEEE*

***Abstract*— In practice, visible light signals undergo non-line-of-sight (NLOS) propagation, and in visible light-based positioning (VLP) methods, the NLOS links are usually treated as disturbance sources to simplify the associated signal processing. However, the impact of NLOS propagation on VLP performance is not fully understood. In this paper, we aim to reveal the performance limits of VLP systems in an NLOS propagation environment via Fisher information analysis. Firstly, the closed-form Cramer-Rao lower bound (CRLB) on the estimation error of user detector (UD) location and orientation is established to shed light on the NLOS-based VLP performance limits. Secondly, the information contribution from the NLOS channel is quantified to gain insights into the effect of the NLOS propagation on the VLP performance. It is shown that VLP can gain additional UD location information from the NLOS channel via leveraging the NLOS propagation knowledge. In other words, the NLOS channel can be exploited to improve VLP performance in addition to the line-of-sight (LOS) channel. The obtained closed-form VLP performance limits can not only provide theoretical foundations for the VLP algorithm design under NLOS propagation, but also provide a performance benchmark for various VLP algorithms.**

***Index Terms*— Visible light-based positioning, visible light communication, NLOS effect, localization performance.**

I. Introduction

VISIBLE light-based positioning (VLP) is envisioned to be an important technique to improve the performance of indoor localization, with the widespread use of light emitting diodes (LEDs) for illumination. The position and orientation angle of a user detector (UD) are critical knowledge for location-based services, such as robotic navigation, autonomous parcel sorting [1], [2] and automatic parking [3]. Hence, VLP has attracted increasing attention in industry and academia [4]. A number of VLP methods using various measurement signals, such as the received signal strength (RSS) of visible light [5]–[18] and the combination of RSS with the angle of arrival (AOA) [19], have been studied. A detailed survey of VLP methods can be found in [20].

Manuscript received October 22, 2019; revised February 16, 2020; accepted March 31, 2020. Date of publication April 21, 2020; date of current version July 10, 2020. The associate editor coordinating the review of this article and approving it for publication was M. S. Alouini. *(Corresponding author: Bingpeng Zhou.)*

Bingpeng Zhou is with the School of Electronics and Communication Engineering, Sun Yat-sen University, Guangzhou 510275, China (e-mail: zhoubp3@mail.sysu.edu.cn).

Yuan Zhuang is with the Sate Key Laboratory of Information Engineering in Surveying, Mapping and Remote Sensing, Wuhan University, Wuhan 430079, China (e-mail: zhy.0908@gmail.com).

Yue Cao is with the School of Computing and Communications, Lancaster University, Lancaster LA1 4YW, U.K. (e-mail: yue.cao@lancaster.ac.uk).

Color versions of one or more of the figures in this article are available online at http://ieeexplore.ieee.org.

Digital Object Identifier 10.1109/TWC.2020.2988001

A. Research Motivation

In practice, visible light signals undergo non-line-of-sight (NLOS) propagation, and there are two strategies to handle the NLOS propagation for VLP. The first is the "NLOS-based VLP method". In addition to the line-of-sight (LOS) channel, the NLOS channel is exploited by this method to hopefully extract more UD location knowledge. Unfortunately, it is established in [21] that the NLOS channel gain is dependent on unknown reflection coefficients and scatterer locations, in addition to the unknown UD location. This will extend the uncertainty set of the VLP problem and hence degrade the VLP performance. Thus, it is theoretically unclear whether or not it is helpful for VLP to exploit NLOS links, and how much performance could be gained from harnessing the NLOS links if it is actually helpful. Hence, it is desired to establish the performance limits of the NLOS-based VLP method. The second is the "LOS-based VLP method". [5]–[18], for example, treat the complex NLOS links as disturbance sources without any information contribution to the VLP. Since the uncertain parameters of the NLOS channel will complicate VLP algorithm design, only the LOS channel is exploited by this method to simplify its signal processing. This LOS-based VLP solution is simple, yet its performance is usually limited, especially in a high SNR environment, in which the NLOS propagation will become a principal error source [22]. Hence, it is non-trivial to establish the effect of the NLOS propagation on the LOS-based VLP performance.

A number of papers have studied the performance analysis of VLP methods, e.g., [22]–[26]. In [14], the Cramer-Rao lower bound (CRLB) is studied for visible light-based ranging, where the LEDs are assumed to radiate downward. Similarly, in [24], the CRLB on ranging errors with a known UD height is derived. In addition to RSS, the performance limit of time-of-arrival-based VLP is studied in [23] and [25]. However, the required assumptions in the above works restrict their application for general cases. In addition, the above works only focus on the LOS-based UD localization error. Hence, the effect of NLOS propagation on the VLP performance is unknown. In [22], the performance limits of LOS channel-based VLP methods under NLOS propagation are studied. The

phenomenon of the unknown NLOS link-caused VLP error floor in high SNR environments is studied using numerical results. However, the associated closed-form analysis is not provided in [22]. In addition, the performance limits of NLOS channel-based VLP methods are fully unknown, and the performance gain from handling the NLOS propagation is not yet understood. A geometry-based stochastic channel modeling for visible light communications is established in [21], which can be employed to quantitatively analyze the effect of the NLOS propagation on the VLP performance.

B. Contributions of This Paper

Motivated by the above research efforts, in this paper, we aim to establish the error performance limits of RSS-based VLP methods under NLOS propagation. Specifically, we aim to answer the following open questions:

- Can the NLOS links contribute to the VLP performance?
- If so, how much performance can be gained from harnessing the NLOS links, and how do the NLOS propagation and system parameters (e.g., transmission distance, SNR and the number of LEDs) affect the VLP performance?
- What is the overall performance limit of RSS-based VLP systems under NLOS propagation?

These questions will be answered via closed-form Fisher information matrix (FIM) analysis, which is challenging due to the complex NLOS modeling. To address this challenge, we extract the structured information in the UD location model. The contributions of this paper are summarized as follows.

- *Performance Analysis of LOS-Based VLP:* We establish the performance limit of the LOS-based VLP method in NLOS propagation environments. Unlike [23]– [25], we obtain the closed-form CRLBs on the UD location and orientation estimate errors, and the effect of the NLOS propagation on the LOS-based VLP performance is also revealed. It is shown that the LOS-based VLP error is affected by the measurement noise and the unknown NLOS links-caused measurement bias. As a result, as the SNR increases, the LOS-based VLP performance will hit an error floor caused by the unknown NLOS links. It should be clarified that, unlike [22], we quantitatively analyze the LOS-based VLP performance limit with closed-form results in this paper, and the NLOS propagation-caused VLP error floor of the LOS-based VLP method in the high SNR region is quantified for the first time.
- *Performance Analysis of NLOS-Based VLP:* We conduct closed-form performance limit analysis of the NLOS-based VLP method. It should be clarified that only the LOS-based VLP method is investigated in [22]. Differently, this paper also studies the NLOS-based VLP method, which exploits both LOS and NLOS channels. It is shown that the NLOS-based VLP performance is totally affected by the measurement noise. Hence, unlike the LOS-based VLP method, the NLOS-based VLP method has no error floor in a high SNR region. Particularly, the information contribution of the NLOS-based VLP method from the NLOS channel is quantified for the first time in this paper. In addition, the effect of system parameters on the NLOS-based VLP performance is also analyzed.
- *Performance Gain of Harnessing NLOS Links:* We obtain the closed-form performance gain of the NLOS-based VLP method (from harnessing the NLOS links) over the LOS-based VLP method. It is shown that the NLOS-based VLP performance gain consists of the information gain from the NLOS channel and the NLOS link-caused information loss in the LOS-based VLP. Our performance analysis result implies that harnessing NLOS links can significantly improve the VLP performance, particularly in a high SNR environment.

The obtained VLP performance limits give a performance benchmark for existing VLP methods and form a foundation for the optimization of VLP systems (e.g., resource allocation).

The remainder of this paper is organized as follows. Section II presents the system model. CRLBs are derived in Section III. The performance gain is analysed in Section IV. Asymptotic performance is revealed in Section V. Numerical results are given in Section VI. Section VII concludes the paper.

II. System Model

In this section, we shall elaborate the VLP system setup, its channel model and the VLP problem we considered.

A. System Setup

We consider a VLP system with M LED transmitters and one UD equipped with photodiodes, as illustrated in Fig. 1. Each LED transmitter is equipped with M_E emitters[1] with diverse orientation angles and different locations within a small area of the LED, where $M_E \geq 1$. Let $\mathbf{p}_{k,m} \in \mathbb{R}^3$ and $\mathbf{v}_{k,m} \in \mathbb{R}^3$ be the known location and the orientation vector, respectively, of the kth emitter of the mth LED,[2] for $k = 1 : M_E$ and $m = 1 : M$. These emitters will act as anchors for the UD localization. Let $\mathbf{x} \in \mathbb{R}^3$ and $\mathbf{u} \in \mathbb{R}^3$ be the unknown UD position and orientation vector, respectively. We assume $\|\mathbf{u}\|_2 = 1$ without loss of generality, where $\| \bullet \|_2$ is the ℓ_2-norm on a vector. Let θ_{FOV} and ϕ_{FOV} be the FOV of the UD and LED emitters, respectively.

B. Diffuse-Scattering Model

We consider a diffuse-scattering model with single-bounce reflection since the signal power of multiple-bounce reflections is very small [21]. We assume that there are $L + 1$ paths between each LED emitter and the UD ($l = 0$ for the LOS paths and $l = 1, \cdots, L$ for NLOS paths). Each single-bounce

[1] An LED array with multiple emitters will be widely adopted in visible light communications for high-rate data transmission [26]–[29]. Hence, an LED array will be commonplace and can be easily achieved in VLP. The case of a single emitter can be covered by our model when $M_E = 1$.

[2] In the following, we use "the (k, m)th emitter" to refer to "the kth emitter of the mth LED transmitter", for brevity.

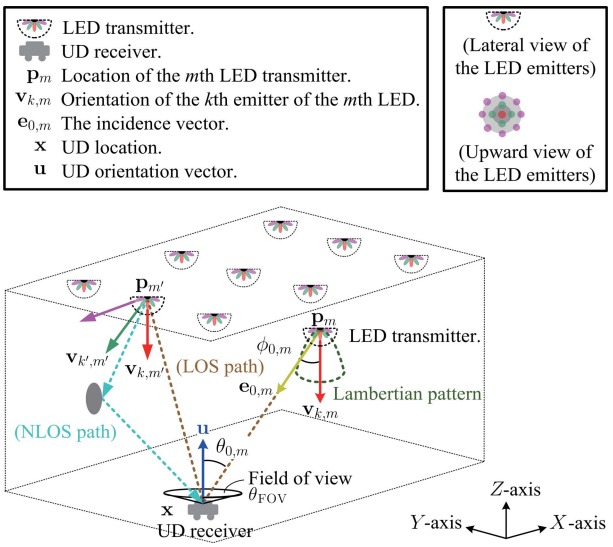

Fig. 1. Illustration of the VLP system.

NLOS link corresponds to one scatterer,[3] as shown in Fig. 2. In addition, we assume the M_E emitters of the same LED are sufficiently close in locations such that they share the same scatterer set.[4] This emitter array will provide diverse location information for alleviating the uncertainties of the NLOS channel. Let $\mathbf{s}_{l,m} \in \mathbb{R}^3$, for $l = 1 : L$, be the unknown scatterer location at the lth path from the mth LED.

Visible light RSS depends on the propagation parameters between the UD and LEDs. Let $\mathbf{e}_{0,k,m} \in \mathbb{R}^3$ be the irradiation vector of the LOS path from the (k,m)th LED emitter to the UD, and let $\mathbf{e}_{l,k,m} \in \mathbb{R}^3$ be the irradiation vector of the NLOS path from the (k,m)th LED emitter to the scatterer $\mathbf{s}_{l,m}$, which are given by

$$\mathbf{e}_{0,k,m} = \frac{\mathbf{x} - \mathbf{p}_{k,m}}{\|\mathbf{x} - \mathbf{p}_{k,m}\|_2}, \tag{1}$$

$$\mathbf{e}_{l,k,m} = \frac{\mathbf{s}_{l,m} - \mathbf{p}_{k,m}}{\|\mathbf{s}_{l,m} - \mathbf{p}_{k,m}\|_2}, \quad \text{for } l = 1 : L. \tag{2}$$

Let $\mathbf{e}'_{l,m} \in \mathbb{R}^3$ be the reflection vector from the lth scatterer to the UD, i.e., $\mathbf{e}'_{l,m} = \dfrac{\mathbf{x} - \mathbf{s}_{l,m}}{\|\mathbf{x} - \mathbf{s}_{l,m}\|_2}$, for $l = 1 : L$.[5] It should be noted that, for the LOS link, the irradiation vector $\mathbf{e}_{0,k,m}$ is identical to the incidence vector of the UD. In addition, let $\rho_{0,k,m}$ be the transmission distance of the LOS path associated with the (k,m)th LED emitter, and let $\rho_{l,k,m}$ be the transmission distance associated with the lth path of the (k,m)th LED emitter, for $l = 1 : L$, namely,

$$\rho_{0,k,m} = \|\mathbf{x} - \mathbf{p}_{k,m}\|_2, \tag{3}$$

$$\rho_{l,k,m} = \|\mathbf{x} - \mathbf{s}_{l,m}\|_2 + \|\mathbf{p}_{k,m} - \mathbf{s}_{l,m}\|_2. \tag{4}$$

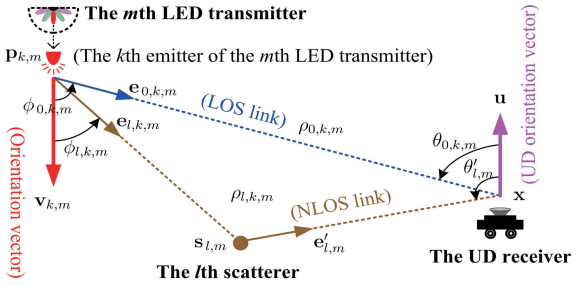

Fig. 2. Illustration of the geometric parameters of diffuse paths.

Let $\phi_{0,k,m}$ be the angle between the (k,m)th LED emitter's orientation vector $\mathbf{v}_{k,m}$ and the irradiance vector $\mathbf{e}_{0,k,m}$, i.e., the LOS-path irradiance angle of the (k,m)th LED emitter, as shown in Fig. 2. Let $\phi_{l,k,m}$ be the angle between the (k,m)th LED emitter's orientation vector $\mathbf{v}_{k,m}$ and the irradiance vector $\mathbf{e}_{l,k,m}$, i.e., the lth NLOS-path irradiance angle of the (k,m)th LED emitter. In addition, let $\theta_{0,k,m}$ be the LOS-path incidence angle between the UD orientation vector $\mathbf{u}$ and the incidence vector $\mathbf{e}_{0,k,m}$, and let $\theta'_{l,m}$, $l = 1 : L$, be the lth NLOS-path incidence angle between the UD orientation vector $\mathbf{u}$ and the reflection vector $\mathbf{e}'_{l,m}$. In a summary, we have

$$\phi_{l,k,m} = \arccos\left(\mathbf{e}_{l,k,m}^{\top}\mathbf{v}_{k,m}\right), \quad \text{for } l = 0 : L, \tag{5}$$

$$\theta_{0,k,m} = \arccos\left(-(\mathbf{e}_{0,k,m})^{\top}\mathbf{u}\right), \tag{6}$$

$$\theta'_{l,m} = \arccos\left(-(\mathbf{e}'_{l,m})^{\top}\mathbf{u}\right), \quad \text{for } l = 1 : L. \tag{7}$$

For the (k,m)th LED emitter, the UD will be able to detect the LOS signal from this LED emitter if the UD is within the FOV angle ϕ_{FOV} of this LED emitter and the LOS-path incidence angle $\theta_{0,k,m}$ is within the FOV angle θ_{FOV} of the UD, *i.e.*, $\left|\frac{\phi_{0,k,m}}{\phi_{\text{FOV}}}\right| \le 1$ and $\left|\frac{\theta_{0,k,m}}{\theta_{\text{FOV}}}\right| \le 1$, where $|\bullet|$ denotes absolute value. Let Ω_R be the set of visible LEDs, and let $\mathbf{s} \in \mathbb{R}^{3L|\Omega_R|}$ be the collection of scatterer locations, given by

$$\Omega_R = \left\{m \middle| \left|\frac{\phi_{0,k,m}}{\phi_{\text{FOV}}}\right| \le 1 \& \left|\frac{\theta_{0,k,m}}{\theta_{\text{FOV}}}\right| \le 1, k = 1 : M_E\right\}, \tag{8}$$

$$\mathbf{s} = \text{vec}[\mathbf{s}_{l,m} | \forall l = 1 : L, \forall m \in \Omega_R], \tag{9}$$

where vec[•] yields a vector by stacking all elements.

C. Visible Light RSS Model

The visible light RSS is fundamentally determined by the transmitter steering gain and the receiver response gain as well as the reflection coefficients (for NLOS links only), which are also related to the above geometric location parameters.

1) Steering Gain of LED Emitter: The LED emitter steering gain depends on the emitting power and irradiation angle. We assume all LED emitters have the same emission-power W_T. The radiation of LED emitters is usually described by a Lambertian pattern [39] characterized by a Lambertian order $r = -\frac{\ln 2}{\ln \cos(A_{\frac{1}{2}})}$, where $A_{\frac{1}{2}}$ is the semi-angle at half power of LED emitters [40]. Then, for the lth path associated with

[3]We consider a discrete reflection model to make a good balance between the model complexity and efficiency, considering the high computational cost of a continuous model [29]– [31]. The continuous reflection from a surface can be treated as the limiting case of our model when $L \to \infty$. Although the number of reflections will be infinite, its power is limited and the reflection coefficient is a finite number, leading to a well-posed VLP problem. Hence, our performance analysis holds for this limiting case.

[4]This is reasonable since the small difference of emitter locations means a similar geometry of emitters with scatterers and the UD, and hence means their similar reflection paths [32]– [38]. The case of different scatterers for emitters can be viewed as a special case of our model, where those emitters associated with different scatterers are treated as different LEDs.

[5]The index k is omitted in $\mathbf{e}'_{l,m}$ for brevity, since the emitters of the same LED share the same scatterer set and thus the reflection vectors from the same scatter of different emitters are the same.

the irradiance angle $\phi_{l,k,m}$, the steering gain of the (k,m)th LED emitter is given by $W_T(r+1)\big(\cos\big(\phi_{l,k,m}\big)\big)^r$ for the unit emission power, where $l=0:L$.

2) Response Gain of UD: The UD response gain depends on the incidence angle and the transmission distance. For the UD photodiode, we assume its aperture, optical filter gain and optical concentrator gain is Φ_R, G_R and Γ_R, respectively, where $\Gamma_R=\frac{\zeta_R^2}{(\sin(\theta_{\rm FOV}))^2}$ in which ζ_R is the refractive index of UD optical concentrator. Hence, the UD response gain associated with the lth incidence angle $\theta'_{l,m}$ and the (k,m)th emitter is given by $\frac{\Gamma_R G_R \Phi_R \cos(\theta'_{l,m})}{2\pi\rho^2_{l,k,m}}$, for $l=1:L$.

3) RSS Model: Based on the above scattering model, the visible light RSS of each path is determined by both the LED steering gain and the UD response gain associated with the transmission distance. Hence, the visible light RSS $\mathrm{z}_{k,m}$ associated with the (k,m)th LED emitter is given by [21]

$$\mathrm{z}_{k,m}=\mathrm{h}_{k,m}(\mathbf{x},\mathbf{u},\mathbf{s})+\epsilon_{k,m}, \tag{10}$$

where $\epsilon_{k,m}$ is the measurement noise. To facilitate the analysis, we assume $\epsilon_{k,m}$ follows a zero-mean Gaussian distribution, i.e., $\epsilon_{k,m}\sim\mathcal{N}(\epsilon_{k,m}|0,\omega)$, $\forall k=1:M_E$, $\forall m\in\Omega_R$, with precision ω (inverse variance). In addition, $\mathrm{h}_{k,m}(\mathbf{x},\mathbf{u},\mathbf{s})=\sum\limits_{l=0:L}\mathrm{h}_{l,k,m}$ is the measurement function, where $\mathrm{h}_{l,k,m}$ is the RSS in the lth NLOS path, given by [21], [30], [42]

$$\mathrm{h}_{0,k,m}=\Psi_R\frac{(r+1)\left(\cos(\phi_{0,k,m})\right)^r\cos(\theta_{0,k,m})}{\|\mathbf{x}-\mathbf{p}_{k,m}\|_2^2}, \tag{11}$$

$$\mathrm{h}_{l,k,m}=\Psi_R\,\wp_{l,m}\eta_k(\mathbf{s}_{l,m})\frac{\cos(\theta_{l,m})}{\|\mathbf{x}-\mathbf{s}_{l,m}\|_2^2},\quad l=1:L, \tag{12}$$

for $k=1:M_E$ and $m\in\Omega_R$, where $\wp_{l,m}\in[0,1)$ represents the reflection coefficient of the lth scatterer associated with the (k,m)th LED emitter, which is an unknown scalar; Ψ_R is a known constant dependent on the aperture, optical filter gain and optical concentrator gain of the UD, given by $\Psi_R=\dfrac{W_T\Gamma_R G_R\Phi_R}{2\pi}$; and $\eta_k(\mathbf{s}_{l,m})\in\mathbb{R}$ is the (unknown) steering gain associated with the transmission distance from the (k,m)th LED emitter to the lth scatterer, given by

$$\eta_k(\mathbf{s}_{l,m})=\frac{(r+1)^2\big(\cos\big(\phi_{l,k,m}\big)\big)^r}{2\pi\|\mathbf{p}_{k,m}-\mathbf{s}_{l,m}\|_2^2},\quad\text{for } l=1:L, \tag{13}$$

where $\phi_{l,m}$ is given by (5).

For ease of notation, let $\boldsymbol{\wp}\in\mathbb{R}^{L|\Omega_R|}=\mathsf{vec}[\wp_{l,m}|\forall l=1:L,\ \forall m\in\Omega_R]$, let $\boldsymbol{\beta}_{\rm UD}\in\mathbb{R}^6=[\mathbf{x};\mathbf{u}]$, let $\boldsymbol{\beta}_{\rm S}\in\mathbb{R}^{4L|\Omega_R|}=[\mathbf{s};\boldsymbol{\wp}]$, and let $\boldsymbol{\alpha}\in\mathbb{R}^{4L|\Omega_R|+6}=[\boldsymbol{\beta}_{\rm UD};\boldsymbol{\beta}_{\rm S}]$ be the joint vector.

As per the relationship between $\{\theta_{l,m},\phi_{l,m}|\forall l=0:L\}$ and $\{\mathbf{x},\mathbf{u},\mathbf{s}\}$ described in (5)–(7), $\mathrm{z}_{k,m}$ is rewritten as

$$\mathrm{z}_{k,m}=\big(\mathbf{g}^{\mathsf{los}}_{k,m}(\mathbf{x})+\mathbf{g}^{\mathsf{nlos}}_{k,m}(\mathbf{x},\boldsymbol{\beta}_{\rm S})\big)^\top\boldsymbol{\mu}(\mathbf{u})+\epsilon_{k,m}, \tag{14}$$

where $\boldsymbol{\mu}(\mathbf{u})=\dfrac{\mathbf{u}}{\|\mathbf{u}\|_2}$, $\mathbf{g}^{\mathsf{los}}_{k,m}(\mathbf{x})$ and $\mathbf{g}^{\mathsf{nlos}}_{k,m}(\mathbf{x},\boldsymbol{\beta}_{\rm S})$ (both in $\mathbb{R}^3$) is the coefficient vector of $\boldsymbol{\mu}(\mathbf{u})$ associated with the LOS link and NLOS link, respectively, given by (15) and (16), as shown at the bottom of this page.

$$\mathbf{g}^{\mathsf{los}}_{k,m}(\mathbf{x})=\Psi_R\frac{(r+1)\left((\mathbf{x}-\mathbf{p}_{k,m})^\top\mathbf{v}_{k,m}\right)^r}{\|\mathbf{x}-\mathbf{p}_{k,m}\|_2^{r+3}}(\mathbf{p}_{k,m}-\mathbf{x}). \tag{15}$$

Let $\mathbf{z}\in\mathbb{R}^{M_E|\Omega_R|}=\mathsf{vec}[\mathrm{z}_{k,m}|\forall k=1:M_E,\forall m\in\Omega_R]$ be the collection of RSS measurements. Then, $\mathbf{z}$ is given by

$$\mathbf{z}=\mathbf{G}(\mathbf{x},\boldsymbol{\beta}_{\rm S})\,\boldsymbol{\mu}(\mathbf{u})+\boldsymbol{\epsilon}, \tag{17}$$

where $\boldsymbol{\epsilon}\in\mathbb{R}^{M_E|\Omega_R|}$ is the noise vector, and the coefficient matrix $\mathbf{G}(\mathbf{x},\boldsymbol{\beta}_{\rm S})\in\mathbb{R}^{M_E|\Omega_R|\times 3}$ is given by

$$\mathbf{G}=\mathrm{mat}\big[\big(\mathbf{g}^{\mathsf{los}}_{k,m}+\mathbf{g}^{\mathsf{nlos}}_{k,m}\big)^\top|\forall k=1:M_E,\forall m\in\Omega_R\big], \tag{18}$$

where $\mathrm{mat}[\bullet]$ yields a matrix by stacking all given row vectors. Let $\mathbf{G}_{\mathsf{los}}$ and $\mathbf{G}_{\mathsf{nlos}}\in\mathbb{R}^{M_E|\Omega_R|\times 3}$ be the coefficient matrix associated with the LOS and NLOS channel, respectively,

$$\mathbf{G}_{\mathsf{los}}=\mathrm{mat}[(\mathbf{g}^{\mathsf{los}}_{k,m}(\mathbf{x}))^\top|\forall k=1:M_E,\forall m\in\Omega_R], \tag{19}$$

$$\mathbf{G}_{\mathsf{nlos}}=\mathrm{mat}[(\mathbf{g}^{\mathsf{nlos}}_{k,m}(\mathbf{x},\boldsymbol{\beta}_{\rm S}))^\top|\forall k=1:M_E,\forall m\in\Omega_R]. \tag{20}$$

D. Problem Formulation of VLP

VLP is to estimate the UD location parameters $(\mathbf{x},\mathbf{u})$ from $\{\mathrm{z}_{k,m}|\forall k=1:M_E,\ \forall m\in\Omega_R\}$, under NLOS propagation with unknown parameters $\{\mathbf{s}_{l,m}|\forall l=1:L,\ \forall m\in\Omega_R\}$ and $\{\wp_{l,m}|\forall l=1:L,\ \forall m\in\Omega_R\}$.

There are two typical methods, based on different assumptions, to solve this VLP problem. The first is the LOS-based VLP method, in which only the LOS channel is exploited and the NLOS channel is assumed to be unknown, as formulated by the following optimization problem,

$$\mathcal{P}_{\mathsf{LOS\text{-}VLP}}:(\hat{\mathbf{x}}_{\mathsf{los}},\hat{\mathbf{u}}_{\mathsf{los}})=\arg\min_{\mathbf{x},\mathbf{u}}\ \|\mathbf{z}-\mathbf{G}_{\mathsf{los}}(\mathbf{x})\boldsymbol{\mu}(\mathbf{u})\|_2^2.$$

The second is the NLOS-based VLP method exploiting both LOS and NLOS channels, which can be formulated as

$$\mathcal{P}_{\mathsf{NLOS\text{-}VLP}}:\quad(\hat{\mathbf{x}}_{\mathsf{nlos}},\hat{\mathbf{u}}_{\mathsf{nlos}})=\arg\min_{\mathbf{x},\mathbf{u}}\ \underbrace{\min\{\|\mathbf{z}-\mathbf{G}(\mathbf{x},\boldsymbol{\beta}_{\rm S})\boldsymbol{\mu}(\mathbf{u})\|_2^2:\forall\boldsymbol{\beta}_{\rm S}\}}_{\text{Cost function }\vartheta(\mathbf{x},\mathbf{u})},$$

where it should be noted that $\vartheta(\mathbf{x},\mathbf{u})$ only depends on the UD location parameters $(\mathbf{x},\mathbf{u})$ but is independent of scattering parameters $\boldsymbol{\beta}_{\rm S}$, since $\vartheta(\mathbf{x},\mathbf{u})$ has been minimized over $\boldsymbol{\beta}_{\rm S}$.

The goal of this paper is to reveal the performance limits of these two VLP methods, i.e., $\mathbb{E}\{\|\hat{\mathbf{x}}_{\mathsf{los}}-\mathbf{x}\|_2^2\}$, $\mathbb{E}\{\|\hat{\mathbf{u}}_{\mathsf{los}}-\mathbf{u}\|_2^2\}$, $\mathbb{E}\{\|\hat{\mathbf{x}}_{\mathsf{nlos}}-\mathbf{x}\|_2^2\}$ and $\mathbb{E}\{\|\hat{\mathbf{u}}_{\mathsf{nlos}}-\mathbf{u}\|_2^2\}$, where $\mathbb{E}\{\bullet\}$ is the expectation over $\mathbf{z}$. We also aim to establish the impact of the NLOS propagation, SNR, transmission distance, reflection coefficient and the number of LEDs on the VLP performance.

Challenge: However, it is challenging to analyze the LOS-based and NLOS-based VLP error performance limits, since there is no closed-form expression of the mean squared VLP

$$\mathbf{g}^{\mathsf{nlos}}_{k,m}(\mathbf{x},\boldsymbol{\beta}_{\rm S})=\Psi_R\sum_{l=1:L}\wp_{l,m}\frac{(r+1)^2\left((\mathbf{p}_{k,m}-\mathbf{s}_{l,m})^\top\mathbf{v}_{k,m}\right)^r}{2\pi\|\mathbf{p}_{k,m}-\mathbf{s}_{l,m}\|_2^{r+2}\|\mathbf{x}-\mathbf{s}_{l,m}\|_2^3}(\mathbf{s}_{l,m}-\mathbf{x}). \tag{16}$$

errors (e.g., $\mathbb{E}\{\|\hat{\mathbf{x}}_{\mathsf{los}}-\mathbf{x}\|_2^2\}$) due to the nonlinear system function with respected to (w.r.t.) $(\mathbf{x}, \mathbf{u})$. □

To address this challenge, we use the inverse matrix lemma [43], [44] for complex FIM functions and the first-order Taylor expansion for nonlinear system models to gain a closed-form CRLB analysis for the VLP error performance.[6]

III. Performance Limits of VLP

To achieve our goal, we first establish the closed-form error bounds (i.e., CRLBs) for the UD location parameter estimates $(\hat{\mathbf{x}}, \hat{\mathbf{u}})$ of the typical VLP methods $\mathcal{P}_{\mathsf{LOS\text{-}VLP}}$ and $\mathcal{P}_{\mathsf{NLOS\text{-}VLP}}$, in turn. Then, we analyze the localization performance gain from harnessing the NLOS links.

A. LOS-Based VLP Performance Limits

We consider the LOS-based VLP method $\mathcal{P}_{\mathsf{LOS\text{-}VLP}}$, where only the LOS channel is exploited. Let $\upsilon_{\mathbf{x}}$ and $\upsilon_{\mathbf{u}}$ be the NLOS channel-caused estimate bias of $\hat{\mathbf{x}}_{\mathsf{los}}$ and $\hat{\mathbf{u}}_{\mathsf{los}}$, respectively,

$$\upsilon_{\mathbf{x}} = \|\mathbb{E}\{\hat{\mathbf{x}}_{\mathsf{los}}\}-\mathbf{x}\|_2, \tag{21}$$

$$\upsilon_{\mathbf{u}} = \|\mathbb{E}\{\hat{\mathbf{u}}_{\mathsf{los}}\}-\mathbf{u}\|_2. \tag{22}$$

In addition, let $\mathfrak{B}_{\mathbf{x}}^{\mathsf{los}}(\mathbf{x},\mathbf{u})$ and $\mathfrak{B}_{\mathbf{u}}^{\mathsf{los}}(\mathbf{x},\mathbf{u}) \in \mathbb{S}^3$ denote the CRLBs on the covariance of $\hat{\mathbf{x}}_{\mathsf{los}}$ and $\hat{\mathbf{u}}_{\mathsf{los}}$, respectively. Then, we have the following theorem to bound the VLP errors.

Theorem 1 (LOS-Based VLP Error Bound): The LOS-based UD location and orientation estimate errors will be bounded from below, respectively, as follows,

$$\mathbb{E}\{\|\hat{\mathbf{x}}_{\mathsf{los}}-\mathbf{x}\|_2^2\} \geq \mathrm{trace}\big(\mathfrak{B}_{\mathbf{x}}^{\mathsf{los}}(\mathbf{x},\mathbf{u})\big)+\upsilon_{\mathbf{x}}^2, \tag{23}$$

$$\mathbb{E}\{\|\hat{\mathbf{u}}_{\mathsf{los}}-\mathbf{u}\|_2^2\} \geq \mathrm{trace}\big(\mathfrak{B}_{\mathbf{u}}^{\mathsf{los}}(\mathbf{x},\mathbf{u})\big)+\upsilon_{\mathbf{u}}^2, \tag{24}$$

where $\mathrm{trace}(\bullet)$ is the matrix trace, and the closed-form CRLB expressions are given, respectively, by

$$\mathfrak{B}_{\mathbf{x}}^{\mathsf{los}} = \big(\omega \mathbf{H}_{\mathsf{los}}(\mathbf{x})\mathbf{U}(\mathbf{u})\mathbf{F}_{\mathsf{los}}(\mathbf{x})\mathbf{U}^{\top}(\mathbf{u})\,\mathbf{H}_{\mathsf{los}}^{\top}(\mathbf{x})\big)^{-1}, \tag{25}$$

$$\mathfrak{B}_{\mathbf{u}}^{\mathsf{los}} = \big(\omega \boldsymbol{\mathcal{R}}(\mathbf{u})\mathbf{G}_{\mathsf{los}}^{\top}(\mathbf{x})\mathbf{V}_{\mathsf{los}}(\mathbf{x},\mathbf{u})\mathbf{G}_{\mathsf{los}}(\mathbf{x})\boldsymbol{\mathcal{R}}^{\top}(\mathbf{u})\big)^{-1}, \tag{26}$$

in which $\mathbf{H}_{\mathsf{los}}(\mathbf{x}) \in \mathbb{R}^{3\times 3M_E|\Omega_R|}$, $\boldsymbol{\mathcal{R}}(\mathbf{u}) \in \mathbb{S}^3$, $\mathbf{F}_{\mathsf{los}}(\mathbf{x}) \in \mathbb{S}^{M_E|\Omega_R|}$ and $\mathbf{U}(\mathbf{u}) \in \mathbb{R}^{3M_E|\Omega_R|\times M_E|\Omega_R|}$ are given by

$$\mathbf{H}_{\mathsf{los}}(\mathbf{x}) = [\mathbf{H}_{0,k,m}|\forall k=1\!:\!M_E, \forall m \in \Omega_R], \tag{27}$$

$$\mathbf{U}(\mathbf{u}) = \mathbf{I}_{M_E|\Omega_R|} \otimes \boldsymbol{\mu}(\mathbf{u}), \tag{28}$$

$$\mathbf{F}_{\mathsf{los}} = \mathbf{I}_{M_E|\Omega_R|} - \mathbf{G}_{\mathsf{los}}(\mathbf{x})\big(\mathbf{G}_{\mathsf{los}}^{\top}(\mathbf{x})\mathbf{G}_{\mathsf{los}}(\mathbf{x})\big)^{-1}\mathbf{G}_{\mathsf{los}}^{\top}(\mathbf{x}), \tag{29}$$

$$\boldsymbol{\mathcal{R}}(\mathbf{u}) = \frac{\|\mathbf{u}\|_2^2\,\mathbf{I}_3 - \mathbf{u}\mathbf{u}^{\top}}{\|\mathbf{u}\|_2^3}, \tag{30}$$

[6]CRLB quantifies the minimum mean squared error that an unbiased estimator can achieve [45]. Hence, we adopt it as the performance metric to study the VLP performance, as widely adopted in signal processing.

in which $\mathbf{I}_3$ is a 3×3 identity matrix, and $\otimes$ is the Kronecker product, and $\mathbf{H}_{0,k,m} \in \mathbb{R}^{3\times 3}$ and $\mathbf{V}_{\mathsf{los}}(\mathbf{x},\mathbf{u}) \in \mathbb{S}^{M_E|\Omega_R|}$ is given by (31) and (32), as shown at the bottom of this page, respectively.

Proof: See the proof in Appendix A. ■

In [22], a CRLB is also obtained, which considers the LOS environment and the UD location estimate. Unlike [22], we consider the NLOS prorogation and the unknown UD orientation and its effect on the UD location estimate performance, leading to a tighter location CRLB $\mathfrak{B}_{\mathbf{x}}^{\mathsf{los}}$. In addition, the closed-form UD orientation CRLB $\mathfrak{B}_{\mathbf{u}}^{\mathsf{los}}$ is obtained in this paper. It is difficult to derive an exact closed-form expression for the LOS-based estimate bias $\upsilon_{\mathbf{x}}$ and $\upsilon_{\mathbf{u}}$, due to the nonlinear system model (17). In the following, we shall approximately characterize the NLOS-link-caused estimate bias $\upsilon_{\mathbf{x}}$ and $\upsilon_{\mathbf{u}}$.

For convenience, let $\boldsymbol{\varsigma}_{\mathsf{nlos}} = \mathbf{G}_{\mathsf{nlos}}(\mathbf{x})\boldsymbol{\mu}(\mathbf{u})$ be the unknown NLOS component of the LOS-based VLP method, let $\boldsymbol{\varsigma}_{\mathsf{bias}}$ be its measurement bias due to $\boldsymbol{\varsigma}_{\mathsf{nlos}}$, and let $\boldsymbol{\varsigma}_{\mathsf{resi}}$ be its residual measurement error (all in $\mathbb{R}^{M_E|\Omega_R|}$), which is given by

$$\boldsymbol{\varsigma}_{\mathsf{resi}} = \mathbf{z} - \mathbf{G}_{\mathsf{los}}(\hat{\mathbf{x}}_{\mathsf{los}})\boldsymbol{\mu}(\hat{\mathbf{u}}_{\mathsf{los}}), \tag{33}$$

where $\hat{\mathbf{x}}_{\mathsf{los}}$ is given in $\mathcal{P}_{\mathsf{LOS\text{-}VLP}}$, and $\mathbf{G}_{\mathsf{los}}(\hat{\mathbf{x}}_{\mathsf{los}})\boldsymbol{\mu}(\hat{\mathbf{u}}_{\mathsf{los}})$ is its measurement estimation. We know from the system model that $\mathbf{z} = \mathbf{G}_{\mathsf{los}}(\mathbf{x})\boldsymbol{\mu}(\mathbf{u}) + \boldsymbol{\varsigma}_{\mathsf{nlos}} + \boldsymbol{\epsilon} = \mathbf{G}_{\mathsf{los}}(\hat{\mathbf{x}}_{\mathsf{los}})\boldsymbol{\mu}(\hat{\mathbf{u}}_{\mathsf{los}}) + \boldsymbol{\varsigma}_{\mathsf{resi}}$. We can observe that there is a measurement bias in the LOS-based VLP method, i.e., $\mathbf{G}_{\mathsf{los}}(\hat{\mathbf{x}}_{\mathsf{los}})\boldsymbol{\mu}(\hat{\mathbf{u}}_{\mathsf{los}}) - \mathbf{G}_{\mathsf{los}}(\mathbf{x})\boldsymbol{\mu}(\mathbf{u})$, denoted by $\boldsymbol{\varsigma}_{\mathsf{bias}} \in \mathbb{R}^{M_E|\Omega_R|}$, where $\mathbf{G}_{\mathsf{los}}(\mathbf{x})\boldsymbol{\mu}(\mathbf{u})$ represents the true measurement without noises. We can also observe that $\boldsymbol{\varsigma}_{\mathsf{bias}}$ mainly stems from $\boldsymbol{\varsigma}_{\mathsf{nlos}}$ and $\boldsymbol{\varsigma}_{\mathsf{resi}}$ since we have assumed the measurement noise $\boldsymbol{\epsilon}$ is zero-mean, which is given by

$$\boldsymbol{\varsigma}_{\mathsf{bias}} = \boldsymbol{\varsigma}_{\mathsf{nlos}} - \boldsymbol{\varsigma}_{\mathsf{resi}}. \tag{34}$$

In the following, we show that the NLOS-caused location estimation bias $\upsilon_{\mathbf{x}}$ and $\upsilon_{\mathbf{u}}$ are entirely determined by $\boldsymbol{\varsigma}_{\mathsf{bias}}$.

Theorem 2 (LOS-Based VLP Bias): The estimate biases $\upsilon_{\mathbf{x}}$ and $\upsilon_{\mathbf{u}}$ in LOS-based VLP are approximately given by

$$\upsilon_{\mathbf{x}} \approx \|\boldsymbol{\varsigma}_{\mathsf{bias}}\|_2 \|\mathbf{H}_{\mathsf{los}}(\mathbf{x})\mathbf{U}(\mathbf{u})\|_2^{-1}, \tag{35}$$

$$\upsilon_{\mathbf{u}} \approx \|\boldsymbol{\varsigma}_{\mathsf{bias}}\|_2 \|\boldsymbol{\mathcal{R}}(\mathbf{u})\mathbf{G}_{\mathsf{los}}^{\top}(\mathbf{x})\|_2^{-1}, \tag{36}$$

and the approximation error is a second-order infinitesimal $\mathcal{O}\big(\|\hat{\mathbf{x}}_{\mathsf{los}}-\mathbf{x}\|_2^2 + \|\hat{\mathbf{u}}_{\mathsf{los}}-\mathbf{u}\|_2^2\big)$, which can be safely ignored.[7]

Proof: See Appendix B. ■

We have the following Corollary to establish the scaling rule of LOS-based estimation bias w.r.t. the measurement bias, which sheds lights on the impact of the unknown NLOS component on the LOS-based VLP error performance.

[7]$f(x) \sim \mathcal{O}(g(x))$ as $x \to \infty$ means there exists a positive number C_1 and a number X_0 such that $|f(x)| \leq C_1|g(x)|$ holds for all $x > X_0$.

$$\begin{aligned}\mathbf{H}_{0,k,m} = {} & \Psi_R\,\rho_{0,k,m}^{-3}(r+3)(r+1)\big(\mathbf{e}_{0,k,m}^{\top}\mathbf{v}_{k,m}\big)^r\mathbf{e}_{0,k,m}\mathbf{e}_{0,k,m}^{\top} - \Psi_R\,\rho_{0,k,m}^{-3}(r+1)\big(\mathbf{e}_{0,k,m}^{\top}\mathbf{v}_{k,m}\big)^r\mathbf{I}_3 \\ & - \Psi_R\,\rho_{0,k,m}^{-3}r(r+1)\big(\mathbf{e}_{0,k,m}^{\top}\mathbf{v}_{k,m}\big)^{r-1}\mathbf{v}_{k,m}\mathbf{e}_{0,k,m}^{\top},\end{aligned} \tag{31}$$

$$\mathbf{V}_{\mathsf{los}}\big(\mathbf{x},\mathbf{u}\big) = \mathbf{I}_{M_E|\Omega_R|} - \mathbf{U}^{\top}(\mathbf{u})\mathbf{H}_{\mathsf{los}}^{\top}(\mathbf{x})\Big(\mathbf{H}_{\mathsf{los}}(\mathbf{x})\mathbf{U}(\mathbf{u})\mathbf{U}^{\top}(\mathbf{u})\mathbf{H}_{\mathsf{los}}^{\top}(\mathbf{x})\Big)^{-1}\mathbf{H}_{\mathsf{los}}(\mathbf{x})\mathbf{U}(\mathbf{u}). \tag{32}$$

Corollary 1 (Scaling Rule of LOS-Based VLP Bias): The LOS-based VLP bias scales with $\|\boldsymbol{\varsigma}_{\mathsf{bias}}\|_2$ as

$$\lim_{\|\boldsymbol{\varsigma}_{\mathsf{bias}}\|_2\to 0}\frac{\upsilon_{\mathbf{x}}}{\|\boldsymbol{\varsigma}_{\mathsf{bias}}\|_2}\approx\|\mathbf{H}_{\mathsf{los}}(\mathbf{x})\mathbf{U}(\mathbf{u})\|_2^{-1},\tag{37}$$

$$\lim_{\|\boldsymbol{\varsigma}_{\mathsf{bias}}\|_2\to 0}\frac{\upsilon_{\mathbf{u}}}{\|\boldsymbol{\varsigma}_{\mathsf{bias}}\|_2}\approx\|\boldsymbol{\mathcal{R}}(\mathbf{u})\mathbf{G}_{\mathsf{los}}^{\top}(\mathbf{x})\|_2^{-1},\tag{38}$$

with an approximation error $\mathcal{O}\big(\|\hat{\mathbf{x}}_{\mathsf{los}}-\mathbf{x}\|_2^2+\|\hat{\mathbf{u}}_{\mathsf{los}}-\mathbf{u}\|_2^2\big)$.

Proof: It directly follows from Theorem 2. ■

We draw the following Remark on the NLOS effect on the performance of the LOS-based VLP method.

Remark 1: This means that the LOS-based VLP bias reduces with the NLOS signal strength, and the reducing rate depends on the LOS channel gain. For a large VLP area, NLOS signals will fade fast due to the long transmission distance. Hence, the NLOS-caused VLP bias will be alleviated in this case. □

Considering that there is no exact closed-form expression of the LOS-based VLP error, we have the following Theorem to establish an approximate mean squared error (AMSE) for the LOS-based VLP, which helps us gain insights into the overall error performance of LOS-based VLP.

Theorem 3 (LOS-Based VLP Error): The LOS-based UD location and orientation errors are approximately characterized, respectively, as follows,

$$\mathbb{E}\{\|\hat{\mathbf{x}}_{\mathsf{los}}-\mathbf{x}\|_2^2\}\approx\big(\|\boldsymbol{\varsigma}_{\mathsf{bias}}\|_2^2+\mathbb{E}\{\|\boldsymbol{\epsilon}\|_2^2\}\big)\|\mathbf{H}_{\mathsf{los}}(\mathbf{x})\mathbf{U}(\mathbf{u})\|_2^{-2},$$
$$\mathbb{E}\{\|\hat{\mathbf{u}}_{\mathsf{los}}-\mathbf{u}\|_2^2\}\approx\big(\|\boldsymbol{\varsigma}_{\mathsf{bias}}\|_2^2+\mathbb{E}\{\|\boldsymbol{\epsilon}\|_2^2\}\big)\|\mathbf{G}_{\mathsf{los}}(\mathbf{x})\boldsymbol{\mathcal{R}}^{\top}(\mathbf{u})\|_2^{-2},$$

with an approximation error of $\mathcal{O}\big(\|\hat{\mathbf{x}}_{\mathsf{los}}-\mathbf{x}\|_2^2+\|\hat{\mathbf{u}}_{\mathsf{los}}-\mathbf{u}\|_2^2\big)$.

Proof: See the proof in APPENDIX C. ■

It is shown that the LOS-based VLP error stems from the measurement noise $\boldsymbol{\epsilon}$ and the NLOS link-caused measurement bias $\boldsymbol{\varsigma}_{\mathsf{bias}}$, and the above Theorem 3 quantifies how these two error sources affect the LOS-based VLP error.

In the following, we reveal how the LOS-based VLP error is quantified. An illustration of the LOS-based VLP error source using the signal projection onto LOS channel-associated measurement space is presented in Fig. 3, where $(\mathbf{x}_{\mathsf{true}},\mathbf{u}_{\mathsf{true}})$ denotes the true value of $(\mathbf{x},\mathbf{u})$, while $\mathbf{x}_{\mathsf{bias}}$ and $\mathbf{x}_{\mathsf{unb}}$ denotes the biased error and unbiased error of LOS-based location estimate $\hat{\mathbf{x}}_{\mathsf{los}}$, given by $\mathbf{x}_{\mathsf{unb}}=\hat{\mathbf{x}}_{\mathsf{los}}-\mathbb{E}\{\hat{\mathbf{x}}_{\mathsf{los}}\}$ and $\mathbf{x}_{\mathsf{bias}}=\mathbb{E}\{\hat{\mathbf{x}}_{\mathsf{los}}\}-\mathbf{x}_{\mathsf{true}}$, respectively, and $\mathbf{z}_{\mathsf{true}}=\mathbf{G}_{\mathsf{los}}(\mathbf{x}_{\mathsf{true}})\boldsymbol{\mu}(\mathbf{u}_{\mathsf{true}})$ denotes the true measurement of the LOS channel. We can see that the LOS-based estimate $(\hat{\mathbf{x}}_{\mathsf{los}},\hat{\mathbf{u}}_{\mathsf{los}})$ corresponds to the sample image $\hat{\mathbf{z}}_{\mathsf{los}}=\mathbf{G}_{\mathsf{los}}(\hat{\mathbf{x}}_{\mathsf{los}})\boldsymbol{\mu}(\hat{\mathbf{u}}_{\mathsf{los}})$ in the range space, which is an orthogonal projection (with the least squared error from $\mathbf{z}$ as formulated in $\mathcal{P}_{\mathsf{LOS\text{-}VLP}}$) of $\mathbf{z}$ onto the LOS channel-associated range space $\mathbb{Z}_{\mathsf{los}}=\{\mathbf{G}_{\mathsf{los}}(\mathbf{x})\boldsymbol{\mu}(\mathbf{u}):\forall\mathbf{x},\forall\mathbf{u}\}$.

Remark 2 (Measurement Error ↦ LOS-Based Range Error): Firstly, the measurement error $\boldsymbol{\epsilon}+\boldsymbol{\varsigma}_{\mathsf{nlos}}$ will lead to a sample image error $\hat{\mathbf{z}}_{\mathsf{los}}-\mathbf{z}_{\mathsf{true}}$ in the LOS-based range space $\mathbb{Z}_{\mathsf{los}}$. Specifically, the sample image error $\hat{\mathbf{z}}_{\mathsf{los}}-\mathbf{z}_{\mathsf{true}}$ stems from the projection of the zero-mean measurement noise $\boldsymbol{\epsilon}$ and the bias measurement error $\boldsymbol{\varsigma}_{\mathsf{bias}}$, i.e., the projection of $\boldsymbol{\varsigma}_{\mathsf{bias}}+\boldsymbol{\epsilon}$, where $\boldsymbol{\varsigma}_{\mathsf{bias}}=\boldsymbol{\varsigma}_{\mathsf{nlos}}-\boldsymbol{\varsigma}_{\mathsf{resi}}$. Hence, the LOS-based location estimation error $\hat{\mathbf{x}}_{\mathsf{los}}-\mathbf{x}_{\mathsf{true}}$ can be cast as the summation of the unbiased error $\mathbf{x}_{\mathsf{unb}}=\hat{\mathbf{x}}_{\mathsf{los}}-\mathbb{E}\{\hat{\mathbf{x}}_{\mathsf{los}}\}$ and the biased error $\mathbf{x}_{\mathsf{bias}}=\mathbb{E}\{\hat{\mathbf{x}}_{\mathsf{los}}\}-\mathbf{x}_{\mathsf{true}}$, which stems from the projection of

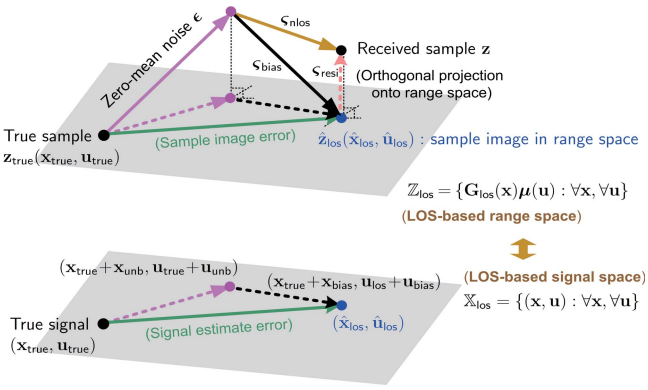

Fig. 3. Illustration of LOS-based VLP error source projection.

the zero-mean measurement error $\boldsymbol{\epsilon}$ and the bias measurement error $\boldsymbol{\varsigma}_{\mathsf{bias}}$, respectively, as shown in Fig. 3 and described in Theorem 3. In addition, since $\boldsymbol{\epsilon}$ is zero-mean, the overall measurement error $\boldsymbol{\varsigma}_{\mathsf{bias}}+\boldsymbol{\epsilon}$ of the LOS channel follows $\mathbb{E}\{\|\boldsymbol{\varsigma}_{\mathsf{bias}}+\boldsymbol{\epsilon}\|_2^2\}=\mathbb{E}\{\|\boldsymbol{\varsigma}_{\mathsf{bias}}\|_2^2\}+\mathbb{E}\{\|\boldsymbol{\epsilon}\|_2^2\}$. □

Remark 3 (LOS-Based Range Error ↦ LOS-Based Estimate Error): Secondly, the LOS-based image error $\hat{\mathbf{z}}_{\mathsf{los}}-\mathbf{z}_{\mathsf{true}}$ leads to the LOS-based VLP error $\|\hat{\mathbf{x}}_{\mathsf{los}}-\mathbf{x}\|_2$. The scaling rate associated with the projection from the LOS-based range space $\mathbb{Z}_{\mathsf{los}}$ to the LOS-based estimator space $\mathbb{X}_{\mathsf{los}}=\{(\mathbf{x},\mathbf{u})|\forall\mathbf{x},\forall\mathbf{u}\}$ is dominated by the first-order Taylor component of the LOS channel function $\mathbf{G}_{\mathsf{los}}(\mathbf{x})\boldsymbol{\mu}(\mathbf{u})$ w.r.t. $(\mathbf{x},\mathbf{u})$ around $(\mathbf{x},\mathbf{u})=(\mathbf{x}_{\mathsf{true}},\mathbf{u}_{\mathsf{true}})$, i.e., $\nabla_{\mathbf{x}}\big(\mathbf{G}(\mathbf{x}_{\mathsf{true}})\boldsymbol{\mu}_{\mathsf{true}}\big)=\mathbf{H}_{\mathsf{los}}(\mathbf{x}_{\mathsf{true}})\mathbf{U}(\mathbf{u}_{\mathsf{true}})$ and $\nabla_{\mathbf{u}}\big(\mathbf{G}(\mathbf{x}_{\mathsf{true}})\boldsymbol{\mu}_{\mathsf{true}}\big)=\boldsymbol{\mathcal{R}}(\mathbf{u}_{\mathsf{true}})\mathbf{G}_{\mathsf{los}}^{\top}(\mathbf{x}_{\mathsf{true}})$. Therefore, the projection of measurement error $\mathbb{E}\{\|\boldsymbol{\varsigma}_{\mathsf{bias}}\|_2^2\}+\mathbb{E}\{\|\boldsymbol{\epsilon}\|_2^2\}$ in the range space onto the signal space should be tuned down by this scaling rate, as described in Theorem 3. □

It is implied by Theorem 3 that, as the SNR increases, the unknown NLOS component will become the dominant localization error source, and hence the LOS-based VLP performance will hit an error floor due to the bias from the non-ignorable NLOS links. We have the following Corollary to characterize this error floor of the LOS-based VLP method.

Corollary 2 (NLOS Link-Caused Error Floor in LOS-Based VLP): As the SNR increases infinitely, the LOS-based VLP error will tend to the following asymptotic limit:

$$\lim_{\mathsf{SNR}\to\infty}\mathbb{E}\{\|\hat{\mathbf{x}}_{\mathsf{los}}-\mathbf{x}\|_2^2\}\approx\mathbb{E}\{\|\boldsymbol{\varsigma}_{\mathsf{bias}}\|_2^2\}\|\mathbf{H}_{\mathsf{los}}(\mathbf{x})\mathbf{U}(\mathbf{u})\|_2^{-2},$$
$$\lim_{\mathsf{SNR}\to\infty}\mathbb{E}\{\|\hat{\mathbf{u}}_{\mathsf{los}}-\mathbf{u}\|_2^2\}\approx\mathbb{E}\{\|\boldsymbol{\varsigma}_{\mathsf{bias}}\|_2^2\}\|\mathbf{G}_{\mathsf{los}}(\mathbf{x})\boldsymbol{\mathcal{R}}^{\top}(\mathbf{u})\|_2^{-2},$$

with an approximation error of $\mathcal{O}\big(\|\hat{\mathbf{x}}_{\mathsf{los}}-\mathbf{x}\|_2^2+\|\hat{\mathbf{u}}_{\mathsf{los}}-\mathbf{u}\|_2^2\big)$.

Proof: As $\mathsf{SNR}\to\infty$, $\|\boldsymbol{\epsilon}\|_2\to 0$, and hence we can obtain the above Corollary 2 as per Theorem 3. ■

This means, the LOS-based VLP error floor is determined by the NLOS links-caused measurement bias $\boldsymbol{\varsigma}_{\mathsf{bias}}$. Unlike LOS-based VLP, NLOS-based VLP will harness NLOS propagation to mitigate its negative effect on the VLP performance. The following performance analysis will show that the NLOS propagation-caused VLP error floor will vanish, by exploiting NLOS propagation knowledge in the UD location estimate.

B. NLOS-Based VLP Performance Limits

In the following, we focus on the performance limit analysis of the NLOS-based VLP exploiting LOS and NLOS channels, which is challenging due to the complex system model.

Theorem 4 (NLOS-Based VLP Error Bound): The NLOS-based UD location and orientation estimate errors will be bounded from below as follows,

$$\mathbb{E}\{\|\hat{\mathbf{x}}_{\mathsf{nlos}}-\mathbf{x}\|_2^2:\boldsymbol{\beta}_{\mathrm{S}}\}\geq \mathrm{trace}\big(\mathfrak{B}_{\mathbf{x}}^{\mathsf{nlos}}(\mathbf{x},\mathbf{u};\boldsymbol{\beta}_{\mathrm{S}})\big), \quad (39)$$

$$\mathbb{E}\{\|\hat{\mathbf{u}}_{\mathsf{nlos}}-\mathbf{u}\|_2^2:\boldsymbol{\beta}_{\mathrm{S}}\}\geq \mathrm{trace}\big(\mathfrak{B}_{\mathbf{u}}^{\mathsf{nlos}}(\mathbf{x},\mathbf{u};\boldsymbol{\beta}_{\mathrm{S}})\big), \quad (40)$$

where $\mathfrak{B}_{\mathbf{x}}^{\mathsf{nlos}}(\mathbf{x},\mathbf{u};\boldsymbol{\beta}_{\mathrm{S}})$ and $\mathfrak{B}_{\mathbf{u}}^{\mathsf{nlos}}(\mathbf{x},\mathbf{u};\boldsymbol{\beta}_{\mathrm{S}})\in\mathbb{S}^3$ denote the NLOS-based location CRLB and orientation CRLB (conditioned on $\boldsymbol{\beta}_{\mathrm{S}}$), respectively, given by[8]

$$\mathfrak{B}_{\mathbf{x}}^{\mathsf{nlos}}=\big(\omega\mathbf{H}(\mathbf{x})\mathbf{U}(\mathbf{u})\mathbf{F}(\mathbf{x})\mathbf{U}^{\top}(\mathbf{u})\mathbf{H}^{\top}(\mathbf{x})-\mathcal{L}_{\mathbf{x}}^{\mathsf{nlos}}(\mathbf{x},\mathbf{u})\big)^{-1},$$
$$\mathfrak{B}_{\mathbf{u}}^{\mathsf{nlos}}=\big(\omega\boldsymbol{\mathcal{R}}(\mathbf{u})\mathbf{G}^{\top}(\mathbf{x})\mathbf{V}\ (\mathbf{x},\mathbf{u})\mathbf{G}(\mathbf{x})\boldsymbol{\mathcal{R}}^{\top}(\mathbf{u})-\mathcal{L}_{\mathbf{u}}^{\mathsf{nlos}}(\mathbf{x},\mathbf{u})\big)^{-1},$$

where $\mathcal{L}_{\mathbf{x}}^{\mathsf{nlos}}(\mathbf{x},\mathbf{u})$ and $\mathcal{L}_{\mathbf{u}}^{\mathsf{nlos}}(\mathbf{x},\mathbf{u})\in\mathbb{S}^3$ denotes the uncertain NLOS channel state-caused information reduction in the UD location and orientation, respectively, which are given later.

Proof: See the proof in APPENDIX D. ■

In addition, $\mathbf{F}(\mathbf{x})\in\mathbb{S}^{M_E|\Omega_R|}$ is given by

$$\mathbf{F}(\mathbf{x})=\mathbf{I}_{M_E|\Omega_R|}-\mathbf{G}(\mathbf{x})\big(\mathbf{G}^{\top}(\mathbf{x})\mathbf{G}(\mathbf{x})\big)^{-1}\mathbf{G}^{\top}(\mathbf{x}), \quad (41)$$

where $\mathbf{G}(\mathbf{x})$ is given in (18), and $\mathbf{V}\ (\mathbf{x},\mathbf{u})\in\mathbb{S}^{M_E|\Omega_R|}$ is given by (42), as shown at the bottom of this page. In addition, $\mathbf{H}(\mathbf{x})\in\mathbb{R}^{3\times 3M_E|\Omega_R|}$ is given by

$$\mathbf{H}(\mathbf{x})=[\mathbf{H}_{k,m}|\forall k=1:M_E,\forall m\in\Omega_R], \quad (43)$$

$$\mathbf{H}_{k,m}=\mathbf{H}_{0,k,m}+\sum_{l=1:L}\mathbf{H}_{l,k,m}, \quad (44)$$

where $\mathbf{H}_{0,k,m}$ is given by (31), and $\mathbf{H}_{l,k,m}\in\mathbb{R}^{3\times 3}$, for $l=1:L$, is given by

$$\mathbf{H}_{l,k,m}=3\Psi_R\frac{(r+1)^2}{2\pi}\frac{\wp_{l,m}\varphi_{l,k,m}(\mathbf{s}_{l,m})}{\|\mathbf{x}-\mathbf{s}_{l,m}\|_2^5}(\mathbf{x}-\mathbf{s}_{l,m})(\mathbf{x}-\mathbf{s}_{l,m})^{\top}-\Psi_R\frac{(r+1)^2}{2\pi}\frac{\wp_{l,m}\varphi_{l,k,m}(\mathbf{s}_{l,m})}{\|\mathbf{x}-\mathbf{s}_{l,m}\|_2^3}\mathbf{I}_3, \quad (45)$$

in which $\varphi_{l,k,m}(\mathbf{s}_{l,m})\in\mathbb{R}$ is given by

$$\varphi_{l,k,m}(\mathbf{s}_{l,m})=\frac{\big((\mathbf{s}_{l,m}-\mathbf{p}_{k,m})^{\top}\mathbf{v}_{k,m}\big)^r}{\|\mathbf{s}_{l,m}-\mathbf{p}_{k,m}\|_2^{r+2}}. \quad (46)$$

In addition, $\mathcal{L}_{\mathbf{x}}^{\mathsf{nlos}}(\mathbf{x},\mathbf{u})$ and $\mathcal{L}_{\mathbf{u}}^{\mathsf{nlos}}(\mathbf{x},\mathbf{u})\in\mathbb{S}^3$ are given by

$$\mathcal{L}_{\mathbf{x}}^{\mathsf{nlos}}=\boldsymbol{\mathcal{P}}_{\mathbf{x}}\mathbf{W}_{\mathbf{x}}^{-1}\boldsymbol{\mathcal{P}}_{\mathbf{x}}^{\top}-\omega\mathbf{H}(\mathbf{x})\mathbf{U}(\mathbf{u})\mathbf{F}^{\perp}(\mathbf{x})\mathbf{U}^{\top}(\mathbf{u})\mathbf{H}^{\top}(\mathbf{x}),$$
$$\mathcal{L}_{\mathbf{u}}^{\mathsf{nlos}}=\boldsymbol{\mathcal{P}}_{\mathbf{u}}\mathbf{W}_{\mathbf{u}}^{-1}\boldsymbol{\mathcal{P}}_{\mathbf{u}}^{\top}-\omega\boldsymbol{\mathcal{R}}(\mathbf{u})\mathbf{G}^{\top}(\mathbf{x})\mathbf{V}^{\perp}(\mathbf{x},\mathbf{u})\mathbf{G}(\mathbf{x})\boldsymbol{\mathcal{R}}^{\top}(\mathbf{u}),$$

[8]For ease of notation, we drop $\boldsymbol{\beta}_{\mathrm{S}}$ in the following notations.

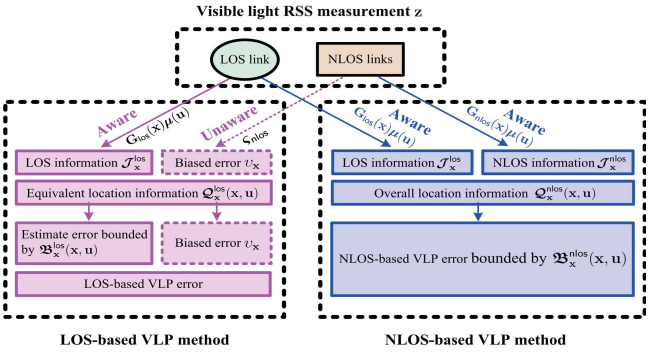

Fig. 4. An illustration of LOS- and NLOS-based VLP information sources.

where $\boldsymbol{\mathcal{P}}_{\mathbf{x}},\boldsymbol{\mathcal{P}}_{\mathbf{u}}\in\mathbb{R}^{3\times(4L|\Omega_R|+3)}$ and $\mathbf{W}_{\mathbf{x}},\mathbf{W}_{\mathbf{u}}\in\mathbb{S}^{(4L|\Omega_R|+3)}$ are given by (105), (109), (106) and (110), respectively, while $\mathbf{F}^{\perp}(\mathbf{x})$ and $\mathbf{V}^{\perp}(\mathbf{x},\mathbf{u})\in\mathbb{S}^{M_E|\Omega_R|}$ are given by

$$\mathbf{F}^{\perp}(\mathbf{x})=\mathbf{I}_{M_E|\Omega_R|}-\mathbf{F}(\mathbf{x}), \quad (47)$$

$$\mathbf{V}^{\perp}(\mathbf{x},\mathbf{u})=\mathbf{I}_{M_E|\Omega_R|}-\mathbf{V}\ (\mathbf{x},\mathbf{u}). \quad (48)$$

We remark on the NLOS-based VLP performance as below.

Remark 4 (Vanished Error Floor of NLOS-Based VLP): It should be noted that the information reduction $\mathcal{L}_{\mathbf{x}}^{\mathsf{nlos}}$ and $\mathcal{L}_{\mathbf{u}}^{\mathsf{nlos}}$ are proportional to ω. Therefore, when $\mathsf{SNR}\to\infty$, the NLOS-based VLP error bound $\mathfrak{B}_{\mathbf{x}}^{\mathsf{nlos}}$ and $\mathfrak{B}_{\mathbf{u}}^{\mathsf{nlos}}$ will approach zero due to the exploitation of the NLOS propagation knowledge in the UD localization, as implied by Theorem 4. Hence, as SNR increases, there is no error floor in the VLP method after exploiting NLOS propagation knowledge. This implies a huge VLP performance gain from harnessing NLOS links. □

In the following, we shall quantify the achieved performance gain of the NLOS-based VLP method (from exploiting the NLOS links) over the LOS-based VLP method.

IV. NLOS-BASED VLP PERFORMANCE GAIN FROM HARNESSING NLOS PROPAGATION

Let us start with the analysis of LOS-based VLP information sources. Then, we will elaborate NLOS-based VLP information sources to reveal the performance gain from harnessing NLOS propagation. An illustration of LOS-based and NLOS-based VLP information sources is provided in Fig. 4.

A. Information Elements of LOS-Based VLP

For convenience, we define the following information notations associated with the LOS-based VLP method $\mathcal{P}_{\mathsf{LOS\text{-}VLP}}$.

- *(LOS Link-Contributed FIM):* Let $\mathcal{J}_{\mathbf{x}}^{\mathsf{los}}(\mathbf{x},\mathbf{u})\in\mathbb{S}^3$ be the UD location information from the LOS link, i.e., the inverse of LOS-based CRLB $\mathfrak{B}_{\mathbf{x}}^{\mathsf{los}}(\mathbf{x},\mathbf{u})$, given by

$$\mathcal{J}_{\mathbf{x}}^{\mathsf{los}}=\omega\mathbf{H}_{\mathsf{los}}(\mathbf{x})\mathbf{U}(\mathbf{u})\mathbf{F}_{\mathsf{los}}(\mathbf{x})\mathbf{U}^{\top}(\mathbf{u})\,\mathbf{H}_{\mathsf{los}}^{\top}(\mathbf{x}), \quad (49)$$

$$\mathbf{V}\ (\mathbf{x},\mathbf{u})=\mathbf{I}_{M_E|\Omega_R|}-\mathbf{U}^{\top}(\mathbf{u})\mathbf{H}^{\top}(\mathbf{x})\big(\mathbf{H}(\mathbf{x})\mathbf{U}(\mathbf{u})\mathbf{U}^{\top}(\mathbf{u})\mathbf{H}^{\top}(\mathbf{x})\big)^{-1}\mathbf{H}(\mathbf{x})\mathbf{U}(\mathbf{u}). \quad (42)$$

where $\mathbf{F}_{\mathsf{los}}(\mathbf{x})$ is given by (29). This FIM quantifies the theoretically maximum information that the LOS-based VLP method can gain from the LOS channel of a clean environment without diffuse scattering (i.e., $\varsigma_{\mathsf{bias}} = 0$).

- *(Equivalent FIM of LOS-Based VLP):* Let $\tilde{\mathcal{Q}}_{\mathbf{x}}^{\mathsf{los}}(\mathbf{x},\mathbf{u}) \in \mathbb{S}^3$ denote the equivalent location FIM (i.e., the accuracy) of the LOS-based VLP method, which is defined as the inverse of the associated error coverable matrix, i.e.,

$$\tilde{\mathcal{Q}}_{\mathbf{x}}^{\mathsf{los}}(\mathbf{x},\mathbf{u}) = \big(\tilde{\mathfrak{B}}_{\mathbf{x}}^{\mathsf{los}}(\mathbf{x},\mathbf{u})\big)^{-1}, \tag{50}$$

where $\tilde{\mathfrak{B}}_{\mathbf{x}}^{\mathsf{los}}(\mathbf{x},\mathbf{u}) \in \mathbb{S}^3$ is the covariance matrix of the LOS-based UD location estimate error, i.e.,

$$\tilde{\mathfrak{B}}_{\mathbf{x}}^{\mathsf{los}}(\mathbf{x},\mathbf{u}) = \mathbb{E}\big\{ (\hat{\mathbf{x}}_{\mathsf{los}} - \mathbf{x}) (\hat{\mathbf{x}}_{\mathsf{los}} - \mathbf{x})^{\top} \big\}. \tag{51}$$

The FIM $\tilde{\mathcal{Q}}_{\mathbf{x}}^{\mathsf{los}}(\mathbf{x},\mathbf{u})$ quantifies the actual net-information gained (from the LOS channel) by the LOS-based VLP method in a diffuse-scattering environment.

- *(Measurement Bias-Caused Equivalent Location FIM):* Let $\mathcal{J}_{\mathbf{x}}^{\mathsf{bias}}(\mathbf{x},\mathbf{u}) \in \mathbb{S}^3$ be the equivalent location FIM associated with the LOS-based location estimation bias caused by the measurement bias $\varsigma_{\mathsf{bias}}$, given by

$$\mathcal{J}_{\mathbf{x}}^{\mathsf{bias}} = \|\varsigma_{\mathsf{bias}}\|_2^{-2} \mathbf{H}_{\mathsf{los}}(\mathbf{x}) \mathbf{U}(\mathbf{u}) \mathbf{U}^{\top}(\mathbf{u}) \mathbf{H}_{\mathsf{los}}^{\top}(\mathbf{x}), \tag{52}$$

where $\varsigma_{\mathsf{bias}}$ is given by (34). This FIM stands for "virtual" information associated with the unknown NLOS links.

Then, we have the following lemma to establish the equivalent information $\tilde{\mathcal{Q}}_{\mathbf{x}}^{\mathsf{los}}(\mathbf{x},\mathbf{u})$ of the LOS-based VLP method.

Lemma 1 (LOS-Based VLP's Equivalent FIM): The equivalent information matrix of the LOS-based VLP method is approximately given by

$$\tilde{\mathcal{Q}}_{\mathbf{x}}^{\mathsf{los}}(\mathbf{x},\mathbf{u}) \approx \underbrace{\Big(\big(\mathcal{J}_{\mathbf{x}}^{\mathsf{los}}(\mathbf{x},\mathbf{u})\big)^{-1} + \big(\mathcal{J}_{\mathbf{x}}^{\mathsf{bias}}(\mathbf{x},\mathbf{u})\big)^{-1} \Big)^{-1}}_{\mathcal{Q}_{\mathbf{x}}^{\mathsf{los}}(\mathbf{x},\mathbf{u})}, \tag{53}$$

with an approximation error of $\mathcal{O}\big(\|\hat{\mathbf{x}}_{\mathsf{los}} - \mathbf{x}\|_2^2 + \|\hat{\mathbf{u}}_{\mathsf{los}} - \mathbf{u}\|_2^2\big)$, where $\mathcal{J}_{\mathbf{x}}^{\mathsf{los}}$ and $\mathcal{J}_{\mathbf{x}}^{\mathsf{bias}}$ is given by (49) and (52), respectively.

Proof: See the proof in APPENDIX E. ∎

Implied by Lemma 1, the LOS-based VLP error follows $\mathbb{E}\big\{(\hat{\mathbf{x}}_{\mathsf{los}} - \mathbf{x})(\hat{\mathbf{x}}_{\mathsf{los}} - \mathbf{x})^{\top}\big\} \approx \big(\mathcal{J}_{\mathbf{x}}^{\mathsf{los}}(\mathbf{x},\mathbf{u})\big)^{-1} + \big(\mathcal{J}_{\mathbf{x}}^{\mathsf{bias}}(\mathbf{x},\mathbf{u})\big)^{-1}$, which is consistent with Theorem 3 and complies with the localization information evolution rule established in [43] and [44]. LOS channel-contributed information $\mathcal{J}_{\mathbf{x}}^{\mathsf{los}}$ is affected by the measurement accuracy ω as shown in (49), whereas the bias information $\mathcal{J}_{\mathbf{x}}^{\mathsf{bias}}$ is determined by the measurement bias strength $\|\varsigma_{\mathsf{bias}}\|_2$ as shown in (52). Hence, the LOS-based VLP error stems from both measurement noise $\boldsymbol{\epsilon}$ and NLOS-caused measurement bias $\varsigma_{\mathsf{bias}}$, as described in (53) and Theorem 3.

The equivalent information $\mathcal{Q}_{\mathbf{x}}^{\mathsf{los}}(\mathbf{x},\mathbf{u})$ describes the LOS-based UD localization accuracy performance limit, i.e., the overall net information under NLOS propagation. It is implied by (53) that the NLOS propogation will lead to an information reduction and hence a performance loss in the LOS-based VLP method, i.e., $\mathcal{Q}_{\mathbf{x}}^{\mathsf{los}} \preceq \mathcal{J}_{\mathbf{x}}^{\mathsf{los}}$. Let $\mathcal{W}_{\mathbf{x}}^{\mathsf{los}} \in \mathbb{S}^3 = \mathcal{J}_{\mathbf{x}}^{\mathsf{los}} - \mathcal{Q}_{\mathbf{x}}^{\mathsf{los}}$ be such NLOS-caused information reduction.

Corollary 3 (Closed-Form Location Information Reduction in LOS-Based VLP): For the LOS-based VLP method, the UD location estimation information reduction due to the unknown NLOS links is given by

$$\mathcal{W}_{\mathbf{x}}^{\mathsf{los}}(\mathbf{x},\mathbf{u}) = \Big(\big(\mathcal{J}_{\mathbf{x}}^{\mathsf{los}}\big)^{-1} \mathcal{J}_{\mathbf{x}}^{\mathsf{bias}} \big(\mathcal{J}_{\mathbf{x}}^{\mathsf{los}}\big)^{-1} + \big(\mathcal{J}_{\mathbf{x}}^{\mathsf{los}}\big)^{-1} \Big)^{-1}, \tag{54}$$

where $\mathcal{J}_{\mathbf{x}}^{\mathsf{los}}$ and $\mathcal{J}_{\mathbf{x}}^{\mathsf{bias}}$ is given by (49) and (52), respectively.

Proof: See the proof in APPENDIX F. ∎

Remark 5 (NLOS-Caused Performance Loss of LOS-Based VLP): We can see from (54) that the information reduction matrix $\mathcal{W}_{\mathbf{x}}^{\mathsf{los}} \succeq \mathbf{0}$, i.e., there must be an information loss in LOS-based VLP due to the NLOS propagation. This is because the unknown NLOS links in RSS measurements behave as disturbance sources for the LOS-based VLP method and hence degrade the achieved VLP performance. Therefore, the LOS channel-based location estimation information will be diluted by the bias information $\mathcal{J}_{\mathbf{x}}^{\mathsf{bias}}$ from $\mathcal{J}_{\mathbf{x}}^{\mathsf{los}}$ to $\mathcal{Q}_{\mathbf{x}}^{\mathsf{los}}$, in a manner described in (53). This complies with our intuition. Ideally, for a clean environment without diffuse scattering, the LOS-based VLP information will be exactly the LOS channel information $\mathcal{J}_{\mathbf{x}}^{\mathsf{los}}(\mathbf{x},\mathbf{u})$ without discount. □

B. Information Sources of NLOS-Based VLP

For the NLOS-based VLP method, since the NLOS propagation knowledge is exploited, there will be information gain from NLOS links. Let $\mathcal{J}_{\mathbf{x}}^{\mathsf{nlos}}(\mathbf{x},\mathbf{u}) \in \mathbb{S}^3$ be the UD location information from the NLOS links (established later). Then, the overall CRLB $\mathfrak{B}_{\mathbf{x}}^{\mathsf{nlos}}(\mathbf{x},\mathbf{u})$ on the NLOS-based UD location estimate error (in Theorem 4) follows

$$\mathfrak{B}_{\mathbf{x}}^{\mathsf{nlos}}(\mathbf{x},\mathbf{u}) = \Big(\underbrace{\mathcal{J}_{\mathbf{x}}^{\mathsf{los}}(\mathbf{x},\mathbf{u}) + \mathcal{J}_{\mathbf{x}}^{\mathsf{nlos}}(\mathbf{x},\mathbf{u})}_{\mathcal{Q}_{\mathbf{x}}^{\mathsf{nlos}}(\mathbf{x},\mathbf{u})} \Big)^{-1}, \tag{55}$$

as illustrated in Fig. 4, where the net information $\mathcal{J}_{\mathbf{x}}^{\mathsf{los}}(\mathbf{x},\mathbf{u})$ from the LOS channel is given by (49), and $\mathcal{Q}_{\mathbf{x}}^{\mathsf{nlos}}(\mathbf{x},\mathbf{u}) \in \mathbb{S}^3$ is the overall information of the NLOS-based VLP, from LOS and NLOS channels. The net information $\mathcal{J}_{\mathbf{x}}^{\mathsf{nlos}}(\mathbf{x},\mathbf{u})$ from the NLOS channel is given by the following Corollary.

Corollary 4 (Location Information From NLOS Links): In the NLOS-based VLP method, the UD location information associated with the NLOS links is given by

$$\mathcal{J}_{\mathbf{x}}^{\mathsf{nlos}}(\mathbf{x},\mathbf{u}) = \mathcal{D}_{\mathbf{x}}^{\mathsf{nlos}}(\mathbf{x},\mathbf{u}) - \mathcal{S}_{\mathbf{x}}^{\mathsf{nlos}}(\mathbf{x},\mathbf{u}), \tag{56}$$

where $\mathcal{D}_{\mathbf{x}}^{\mathsf{nlos}}(\mathbf{x},\mathbf{u}) \in \mathbb{S}^3$ is the raw cross information from the LOS link and NLOS links, given by (57), as shown at the bottom of the next page, where $\mathbf{H}_{\mathsf{nlos}}(\mathbf{x}) \in \mathbb{R}^{3\times 3M_E|\Omega_R|}$ is given by

$$\mathbf{H}_{\mathsf{nlos}}(\mathbf{x}) = \Big[\sum_{l=1:L} \mathbf{H}_{l,k,m} | \forall k = 1{:}M_E, \forall m \in \Omega_R \Big], \tag{58}$$

and $\mathcal{S}_{\mathbf{x}}^{\mathsf{nlos}}(\mathbf{x},\mathbf{u}) \in \mathbb{S}^3$ is the unknown NLOS channel state-caused information reduction, given by

$$\mathcal{S}_{\mathbf{x}}^{\mathsf{nlos}} = \mathcal{P}_{\mathbf{x}} \mathbf{W}_{\mathbf{x}}^{-1} \mathcal{P}_{\mathbf{x}}^{\top} - \omega \mathbf{H}_{\mathsf{los}}(\mathbf{x}) \mathbf{U}(\mathbf{u}) \mathbf{F}_{\mathsf{los}}^{\perp}(\mathbf{x}) \mathbf{U}^{\top}(\mathbf{u}) \mathbf{H}_{\mathsf{los}}^{\top}(\mathbf{x}),$$

in which $\mathcal{P}_{\mathbf{x}}$ and $\mathbf{W}_{\mathbf{x}}$ is given by (105) and (106), respectively, while $\mathbf{F}_{\mathsf{los}}^{\perp}(\mathbf{x})$ is given by

$$\mathbf{F}_{\mathsf{los}}^{\perp}(\mathbf{x}) = \mathbf{G}_{\mathsf{los}}(\mathbf{x}) \big(\mathbf{G}_{\mathsf{los}}^{\top}(\mathbf{x}) \mathbf{G}_{\mathsf{los}}(\mathbf{x}) \big)^{-1} \mathbf{G}_{\mathsf{los}}^{\top}(\mathbf{x}). \tag{59}$$

Proof: See the proof in APPENDIX G. ∎

Corollary 4 quantifies the location information $\boldsymbol{\mathcal{J}}_{\mathbf{x}}^{\mathsf{nlos}}(\mathbf{x},\mathbf{u})$ of the NLOS-based VLP from the NLOS channel. We can observe that the NLOS channel with a well-defined NLOS propagation model can be exploited to extract additional UD location knowledge if $\boldsymbol{\mathcal{J}}_{\mathbf{x}}^{\mathsf{nlos}}(\mathbf{x},\mathbf{u}) \succeq \mathbf{0}$ is satisfied.

C. Performance Gain of NLOS-Based VLP

We shall establish the performance gain of NLOS-based VLP over LOS-based VLP. Let the approximate error $\breve{\boldsymbol{\mathcal{B}}}_{\mathbf{x}}^{\mathsf{los}} = \left(\boldsymbol{\mathcal{Q}}_{\mathbf{x}}^{\mathsf{los}}\right)^{-1}$ (with $\boldsymbol{\mathcal{Q}}_{\mathbf{x}}^{\mathsf{los}}$ given by (53)) represent the error performance limit of the LOS-based VLP method.

Compared with the NLOS-based and the LOS-based VLP information formation in (55) and (53), respectively, we can observe that the NLOS links impose a negative effect on the LOS-based VLP (leading to an information reduction $\boldsymbol{\mathcal{W}}_{\mathbf{x}}^{\mathsf{los}}$) while a positive effect on the NLOS-based VLP (leading to an information gain $\boldsymbol{\mathcal{J}}_{\mathbf{x}}^{\mathsf{nlos}}$). Hence, the overall performance gain of the NLOS-based VLP over the LOS-based VLP includes two parts: the NLOS link-contributed information gain $\boldsymbol{\mathcal{J}}_{\mathbf{x}}^{\mathsf{nlos}}$ and the NLOS link-caused information reduction $\boldsymbol{\mathcal{W}}_{\mathbf{x}}^{\mathsf{los}}$ in the LOS-based VLP method, as elaborated below.

Corollary 5 (NLOS-Based VLP Information Gain Over LOS-Based VLP): The performance gain of NLOS-based VLP over LOS-based VLP, from harnessing NLOS links, is given by

$$\boldsymbol{\mathcal{Q}}_{\mathbf{x}}^{\mathsf{gain}}(\mathbf{x},\mathbf{u}) = \boldsymbol{\mathcal{W}}_{\mathbf{x}}^{\mathsf{los}}(\mathbf{x},\mathbf{u}) + \boldsymbol{\mathcal{J}}_{\mathbf{x}}^{\mathsf{nlos}}(\mathbf{x},\mathbf{u}), \tag{60}$$

where $\boldsymbol{\mathcal{W}}_{\mathbf{x}}^{\mathsf{los}}$ and $\boldsymbol{\mathcal{J}}_{\mathbf{x}}^{\mathsf{nlos}}$ is given by (54) and (56), respectively.

Proof: This Corollary directly follows from the associated definition that $\boldsymbol{\mathcal{Q}}_{\mathbf{x}}^{\mathsf{gain}}(\mathbf{x},\mathbf{u}) = \boldsymbol{\mathcal{Q}}_{\mathbf{x}}^{\mathsf{nlos}}(\mathbf{x},\mathbf{u}) - \boldsymbol{\mathcal{Q}}_{\mathbf{x}}^{\mathsf{los}}(\mathbf{x},\mathbf{u}) = \boldsymbol{\mathcal{J}}_{\mathbf{x}}^{\mathsf{nlos}} + \underbrace{\boldsymbol{\mathcal{J}}_{\mathbf{x}}^{\mathsf{los}} - \left(\left(\boldsymbol{\mathcal{J}}_{\mathbf{x}}^{\mathsf{los}}\right)^{-1} + \left(\boldsymbol{\mathcal{J}}_{\mathbf{x}}^{\mathsf{bias}}\right)^{-1}\right)^{-1}}_{\boldsymbol{\mathcal{W}}_{\mathbf{x}}^{\mathsf{los}}}$. ∎

Then, the following theorem establishes that harnessing the NLOS links will contribute to VLP, if the NLOS-associated information gain $\boldsymbol{\mathcal{J}}_{\mathbf{x}}^{\mathsf{nlos}}$ satisfies a certain condition.

Theorem 5 (Lower Error of NLOS-Based VLP): The NLOS-based VLP error bound is lower than the approximate LOS-based VLP error, i.e., $\mathfrak{B}_{\mathbf{x}}^{\mathsf{nlos}} \preceq \breve{\boldsymbol{\mathcal{B}}}_{\mathbf{x}}^{\mathsf{los}}$, if the following non-negative-gain condition is satisfied,

$$\boldsymbol{\mathcal{Q}}_{\mathbf{x}}^{\mathsf{gain}}(\mathbf{x},\mathbf{u}) \succeq \mathbf{0}_{3\times 3}. \tag{61}$$

Proof: It can be easily verified from (60) that, if (61) is satisfied, we have $\boldsymbol{\mathcal{Q}}_{\mathbf{x}}^{\mathsf{gain}} \succeq \mathbf{0}_{3\times 3}$. Then, based on (55) and (53) in Lemma 1, we finally arrive at $\mathfrak{B}_{\mathbf{x}}^{\mathsf{nlos}} \preceq \breve{\boldsymbol{\mathcal{B}}}_{\mathbf{x}}^{\mathsf{los}}$. ∎

It should be noted that condition (61) is satisfied almost surely. This is because the NLOS link with a well-defined propagation model indeed has useful UD location information, and meanwhile the unknown NLOS link-caused information reduction in the LOS-based VLP method is non-ignorable, i.e., $\boldsymbol{\mathcal{W}}_{\mathbf{x}}^{\mathsf{los}} \succeq \mathbf{0}$. Hence, it is possible to improve the VLP performance via exploiting UD location knowledge from the NLOS links, given the NLOS propagation model. Yet, this is challenging due to the non-convex nature of NLOS-based VLP, and hence it calls for an efficient algorithm design.

V. Asymptotic Performance Analysis

We can see from Theorem 4 that the NLOS-based VLP error is affected by several system parameters, e.g., the transmission distance, SNR and the number of visible LED emitters. In this section, we shall reveal the effect of these critical parameters on the performance of the NLOS-based VLP method.

Firstly, regarding the scaling rule of the NLOS-based CRLB w.r.t. SNR, we have the following Corollary.

Corollary 6 (The Effect of SNR): The NLOS-based VLP error bounds $\mathfrak{B}_{\mathbf{x}}^{\mathsf{nlos}}(\mathbf{x},\mathbf{u})$ and $\mathfrak{B}_{\mathbf{u}}^{\mathsf{nlos}}(\mathbf{x},\mathbf{u})$ scale with the SNR in the following manner, as $\mathsf{SNR} \to \infty$,[9]

$$\mathrm{trace}\left(\mathfrak{B}_{\mathbf{x}}^{\mathsf{nlos}}(\mathbf{x},\mathbf{u})\right) \sim \Theta(\mathsf{SNR}^{-1}), \tag{62}$$

$$\mathrm{trace}\left(\mathfrak{B}_{\mathbf{u}}^{\mathsf{nlos}}(\mathbf{x},\mathbf{u})\right) \sim \Theta(\mathsf{SNR}^{-1}). \tag{63}$$

Proof: It directly follows from Theorem 4. It should be noted that $\boldsymbol{\mathcal{L}}_{\mathbf{x}}^{\mathsf{nlos}}(\mathbf{x},\mathbf{u})$ and $\boldsymbol{\mathcal{L}}_{\mathbf{u}}^{\mathsf{nlos}}(\mathbf{x},\mathbf{u})$ are $\Theta(\mathsf{SNR}^{-1})$, which can be easily verified by their closed-form expressions. ∎

This Corollary implies that the NLOS-based VLP error is totally affected by measurement noise strength, and it reduces with the SNR. Hence, unlike the LOS-based VLP method, the NLOS-based VLP method will no longer have a NLOS-caused error floor in a high-SNR region due to the harnessing of NLOS links. This complies with Remark 4.

For ease of notation, let $\rho_{\min} = \min\{\rho_{k,l,m} | \forall l = 0:L,\ \forall k = 1:M_E,\ \forall m \in \Omega_R\}$ be the minimum transmission distance between the LEDs and the UD.

Secondly, for the scaling rule of the NLOS-based VLP error CRLB w.r.t. the transmission distance between the LED and UD, we have the following conclusion.

Corollary 7 (The Effect of Transmission Distance): The NLOS-based VLP error bounds scale with the transmission distance between the LED and UD as follows,[10] as $\rho_{\min} \to \infty$:

$$\mathrm{trace}\left(\mathfrak{B}_{\mathbf{x}}^{\mathsf{nlos}}(\mathbf{x},\mathbf{u})\right) \sim \Omega(\rho_{\min}^{6}), \tag{64}$$

$$\mathrm{trace}\left(\mathfrak{B}_{\mathbf{u}}^{\mathsf{nlos}}(\mathbf{x},\mathbf{u})\right) \sim \Omega(\rho_{\min}^{4}). \tag{65}$$

Proof: See Appendix H. ∎

This indicates that the NLOS-based location estimate error is increasing with the transmission distance in the sixth power, while the orientation estimate error is increasing with the transmission distance in the fourth power, which is fundamentally determined by the physical propagation model of visible light signals. This means that a larger area needs more LEDs to preserve a satisfactory VLP performance.

Thirdly, for the scaling of the NLOS-based VLP error CRLB w.r.t. the number of LEDs, we have the following conclusion.

[9] $f(x) \sim \Theta(g(x))$ as $x \to \infty$ means there exists C_1, $C_2 > 0$ and a constant X_0 such that $C_1|g(x)| \le |f(x)| \le C_2|g(x)|$ holds for all $x > X_0$.

[10] $f(x) \sim \Omega(g(x))$ as $x \to \infty$ means there exists a positive number C_2 and a number X_0 such that $|f(x)| \ge C_2|g(x)|$ holds for all $x > X_0$.

$$\boldsymbol{\mathcal{D}}_{\mathbf{x}}^{\mathsf{nlos}}(\mathbf{x},\mathbf{u}) = \omega \mathbf{H}_{\mathsf{nlos}}(\mathbf{x})\mathbf{U}(\mathbf{u})\mathbf{U}^{\top}(\mathbf{u})\mathbf{H}_{\mathsf{los}}^{\top}(\mathbf{x}) + \omega \mathbf{H}_{\mathsf{los}}(\mathbf{x})\mathbf{U}(\mathbf{u})\mathbf{U}^{\top}(\mathbf{u})\mathbf{H}_{\mathsf{nlos}}^{\top}(\mathbf{x}) + \omega \mathbf{H}_{\mathsf{nlos}}(\mathbf{x})\mathbf{U}(\mathbf{u})\mathbf{U}^{\top}(\mathbf{u})\mathbf{H}_{\mathsf{nlos}}^{\top}(\mathbf{x}). \tag{57}$$

Corollary 8 (The Effect of LED Set Size): We assume that the LEDs are uniformly distributed within the room. Then, as $|\Omega_R| \to \infty$, the NLOS-based error bounds follows

$$\mathrm{trace}\big(\mathfrak{B}_{\mathbf{x}}^{\mathsf{nlos}}(\mathbf{x},\mathbf{u})\big) \sim \Theta(|\Omega_R|^{-1}), \tag{66}$$

$$\mathrm{trace}\big(\mathfrak{B}_{\mathbf{u}}^{\mathsf{nlos}}(\mathbf{x},\mathbf{u})\big) \sim \Theta(|\Omega_R|^{-1}). \tag{67}$$

Proof: See APPENDIX I. ∎

This means that the NLOS-based VLP error reduces with the number of independent sources, at the rate of $\Theta(|\Omega_R|^{-1})$. Corollaries 7 and 8 can be used to assess how many LED sources are needed to achieve the desired VLP performance.

Fourthly, for the impact of scatterer reflection coefficients on the NLOS-based and LOS-based VLP performance, separately, we have the following Corollaries.

Corollary 9 (The Effect of Reflection Coefficient on NLOS-Based VLP Performance): The NLOS-based VLP error bounds $\mathfrak{B}_{\mathbf{x}}^{\mathsf{nlos}}(\mathbf{x},\mathbf{u})$ and $\mathfrak{B}_{\mathbf{u}}^{\mathsf{nlos}}(\mathbf{x},\mathbf{u})$ scale with the NLOS-path reflection coefficient as follows, as $\|\wp\|_2 \to \infty$:[11]

$$\mathrm{trace}\big(\mathfrak{B}_{\mathbf{x}}^{\mathsf{nlos}}(\mathbf{x},\mathbf{u})\big) \sim \Theta(\|\wp\|_2^{-2}), \tag{68}$$

$$\mathrm{trace}\big(\mathfrak{B}_{\mathbf{u}}^{\mathsf{nlos}}(\mathbf{x},\mathbf{u})\big) \sim \Theta(\|\wp\|_2^{-2}). \tag{69}$$

Corollary 10 (The Effect of Reflection Coefficient on LOS-Based VLP Performance): The LOS-based VLP error bounds $\mathfrak{B}_{\mathbf{x}}^{\mathsf{los}}(\mathbf{x},\mathbf{u})$ and $\mathfrak{B}_{\mathbf{u}}^{\mathsf{los}}(\mathbf{x},\mathbf{u})$ scale with the reflection coefficient strength $\|\wp\|_2$ in the following manner, as $\|\wp\|_2 \to \infty$:

$$\mathrm{trace}\big(\mathfrak{B}_{\mathbf{x}}^{\mathsf{los}}(\mathbf{x},\mathbf{u})\big) \sim \Theta(\|\wp\|_2^{2}), \tag{70}$$

$$\mathrm{trace}\big(\mathfrak{B}_{\mathbf{u}}^{\mathsf{los}}(\mathbf{x},\mathbf{u})\big) \sim \Theta(\|\wp\|_2^{2}). \tag{71}$$

Proof: See APPENDIX J. ∎

We can observe that, when the reflection coefficient increases, the LOS-based VLP error increases accordingly, while the NLOS-based VLP error reduces, both at a second-order rate (considering squared errors), which are totally opposite behaviors. This is because of the different mechanisms for handling the NLOS channel and hence different information structures of these two VLP methods.

The scatterer reflection coefficient will affect the strength of NLOS signals $\|\varsigma_{\mathsf{nlos}}\|_2$, which will further affect the NLOS propagation-caused equivalent information $\mathcal{J}_{\mathbf{x}}^{\mathsf{bias}}(\mathbf{x},\mathbf{u})$ of the LOS-based VLP method (see (52)) and the NLOS channel-contributed information $\mathcal{J}_{\mathbf{x}}^{\mathsf{nlos}}(\mathbf{x},\mathbf{u})$ of the NLOS-based VLP method (see (56)). Yet, $\mathcal{J}_{\mathbf{x}}^{\mathsf{bias}}(\mathbf{x},\mathbf{u})$ leads to an effect of information reduction to the LOS-based VLP method (see (53)), while $\mathcal{J}_{\mathbf{x}}^{\mathsf{nlos}}(\mathbf{x},\mathbf{u})$ leads to an effect of information increase to the NLOS-based VLP method (see (55)). Hence, the reflection coefficient has an entirely different impact on these two VLP methods. Specifically, for the LOS-based VLP method, a small reflection coefficient leads to a small interference and hence a small NLOS-caused error floor and finally a small VLP error. On the contrary, for the NLOS-based VLP method, a small reflection coefficient leads to a small information contribution from the NLOS channel, thus leading to a large VLP error.

[11]Despite $\|\wp\|_2 \in (0,1)$, the following asymptotic limits over $\|\wp\|_2 \to \infty$ are useful for understanding the scaling rule of VLP performance. For $\|\wp\|_2 \to 0$, the LOS-based VLP performance can be directly implied by Theorem 2 and 3. In addition, NLOS-based VLP will reduce to LOS-based VLP in such a case, which means identical performance limits of them.

VI. NUMERICAL RESULTS

We shall use numeric simulations to examine our theoretical results of LOS- and NLOS-based VLP performance limits.

A. Simulation Settings

We consider $M = 15$ LED transmitters uniformly installed on the ceiling of a room with the size of $9[\mathrm{m}] \times 9[\mathrm{m}] \times 4[\mathrm{m}]$. In addition, we assume there are $M_E = 25$ emitters associated with each LED transmitter, which are uniformly distributed within a circle area of $1[\mathrm{cm}^2]$ around the LED transmitter centre. The orientation of all LED emitters is assumed to be with a downwards direction with an arbitrary azimuth direction and a random polar angle. The UD appears in the room at a random location and with a random orientation. In addition, we assume $\Phi_R = 0.5\,[\mathrm{cm}^2]$, $r = 1$, $G_R = 1$, $\Gamma_R = 2.25$, and $\theta_{\mathrm{FOV}} = \phi_{\mathrm{FOV}} = \pi/2$. These parameter settings follow from a typical LED setup that is widely adopted in papers such as [5], [12], [46], [47]. Furthermore, we consider the measurement noise strength to be 10^{-8} such that the SNR is around 30 [dB], and we set $L = 4$ diffuse paths between each LED emitter and the UD [41], unless specified otherwise. The four scatterers between each LED transmitter and UD are randomly distributed within the room since we assume that there is no prior knowledge of scatterer locations. This assumption is general and reasonable in practice. Moreover, we set $\wp_{l,m}$ in (0, 0.8) at random, for each diffuse link.

B. Result Analysis

1) The Effect of SNR: The performance of the LOS- and NLOS-based VLP methods v.s. SNR is shown in Fig. 5, where the measurement noise power reduces such that the SNR varies from -20 [dB] to 80 [dB]. It is shown that, as SNR increases, the LOS-based VLP error reduces and finally hits an error floor in the high SNR region, due to NLOS propagation, which complies with Corollary 2. This means that the NLOS links will become the dominant error of the LOS-based VLP method in high SNR conditions, and hence an advanced VLP algorithm to harness the NLOS links is desired. In contrast, the NLOS-based VLP error reduces as the SNR increases, due to the exploitation of NLOS propagation knowledge, as revealed in Theorem 4 and Corollary 6.

We consider two UD paths, as shown in Fig. 6, to evaluate the associated NLOS-based VLP performance. We can see from Fig. 7 that the VLP will achieve better performance when the UD height is lower than 3[m] for a 4[m]-high room, due to the better sight. In addition, the VLP has a larger error when the UD is closer to the wall.

2) Gain From Harnessing the NLOS Links: The achieved localization performance gain from exploiting NLOS propagation knowledge is shown in Fig. 8, where the associated performance gain of the UD location estimate is defined as the ratio between the LOS-based approximate VLP error $\mathrm{trace}\big(\breve{\mathfrak{B}}_{\mathbf{x}}^{\mathsf{los}}\big)$ and the NLOS-based VLP error bound $\mathrm{trace}\big(\mathfrak{B}_{\mathbf{x}}^{\mathsf{nlos}}\big)$. It is shown that this performance gain increases with SNR. In the high SNR region, the NLOS interference will become the dominant error source. Hence, the VLP method will achieve a

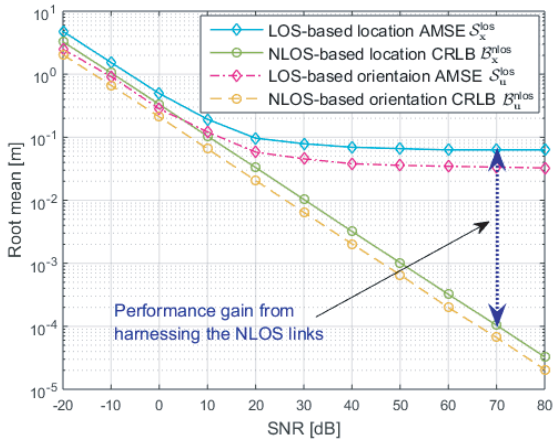

Fig. 5. VLP error performance v.s. SNR.

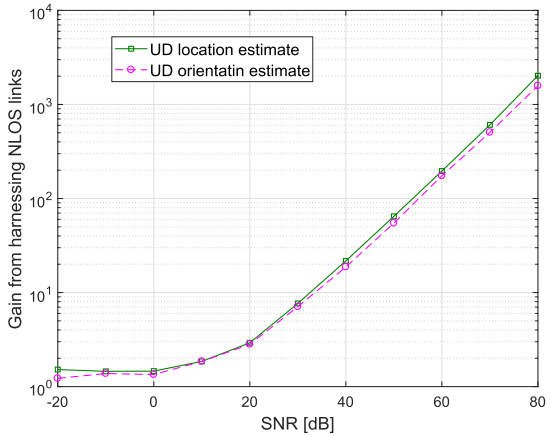

Fig. 8. The performance gain from NLOS links v.s. SNR.

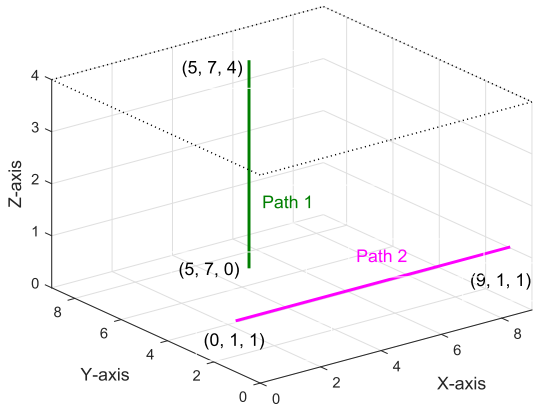

Fig. 6. Illustration of UD paths.

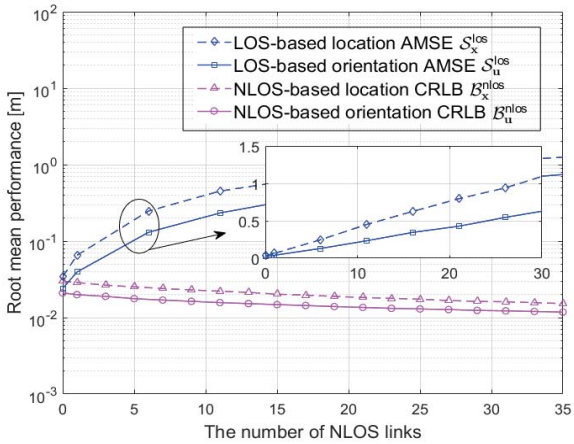

Fig. 9. VLP error performance v.s. the number of NLOS links.

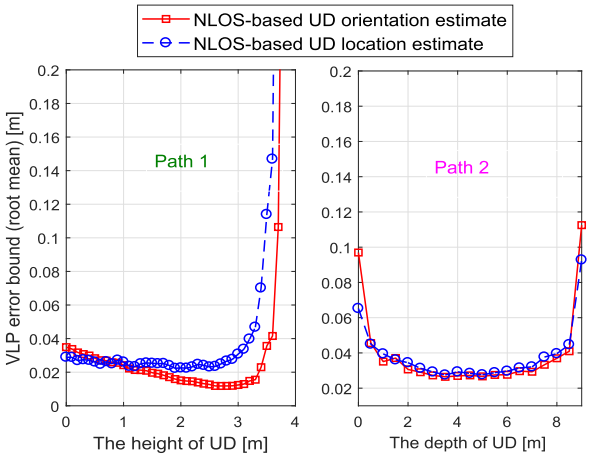

Fig. 7. VLP performance associated with different UD paths.

large performance gain from harnessing the NLOS links. This numerical result complies with Corollary 5 and Theorem 5.

3) The Effect of NLOS Propagation: The LOS- and NLOS-based VLP error performances v.s. the number of NLOS links are given in Fig. 9. It is shown that a larger number of the NLOS links leads to a larger localization error for the LOS-based VLP method, which complies with Corollary 10. In contrast, for the NLOS-based VLP method, the localization error will slightly reduce with the number of NLOS links since more NLOS links bring more UD location information to VLP, which complies with Corollary 9. This means that the NLOS-based VLP method can be expected to achieve a reliable solution in diffuse scattering environments via exploiting NLOS propagation knowledge.

4) The Impact of Reflection Coefficients: The localization performances of LOS- and NLOS-based VLP methods v.s. the reflection coefficients $\{\wp_{l,m}\}$ of NLOS channels are presented in Fig. 10, where we set $\wp_{l,m}$ ranges within [0.1,1) for all NLOS paths. It is shown that the LOS-based VLP error increases (almost linearly) with the reflection coefficient of the NLOS links. This is because a large refection coefficient leads to a large unknown NLOS component, as revealed in Theorem 2, 3 and Corollary 10. In contrast, the NLOS-based VLP error will not increase with an increasing reflection coefficient, due to the exploitation of NLOS propagation knowledge, which complies with Corollary 9.

5) The Effect of the Room Size: The VLP error performance v.s. the room size is presented in Fig. 11, where we consider a cubic room with a length ranging from 5[m] to 100[m] and the LEDs are uniformly distributed on the room ceiling. The

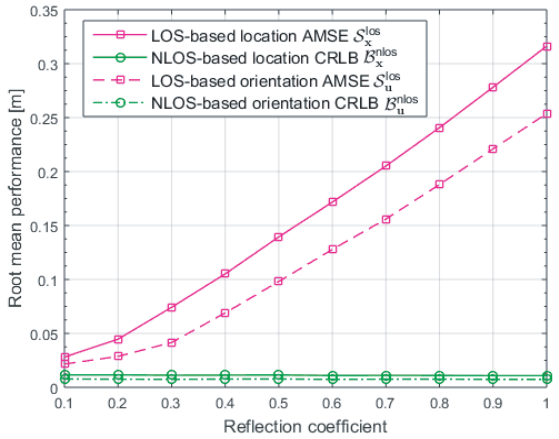

Fig. 10. VLP error performance v.s. the NLOS link's reflection coefficient.

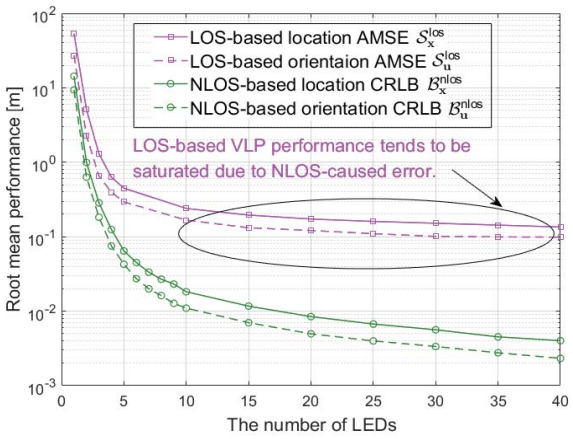

Fig. 12. The impact of the number of LEDs on localization performance.

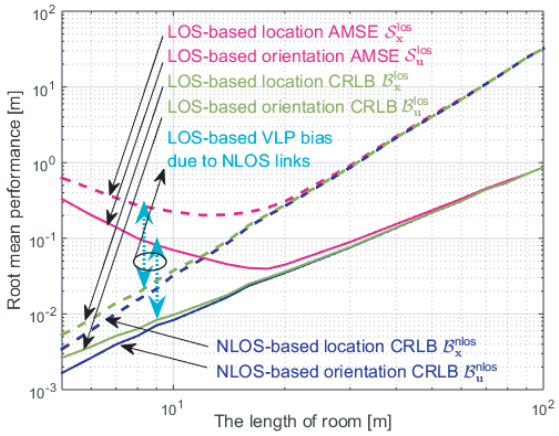

Fig. 11. VLP error performance v.s. the length of the cubic room.

number of LEDs is fixed at 15. It is shown in Fig. 11 that the NLOS-based VLP error increases with the room size, which complies with Corollary 7. In contrast, the LOS-based VLP error first reduces and then increases with the room size. This is because a small NLOS path length will lead to a large NLOS interference, thus rendering a large VLP error, when the room size is small (e.g., less than 10 [m]).[12] As the room size increases, the NLOS path length increases, and hence the NLOS interference will rapidly reduce, so does the gap between the LOS-based VLP error with its CRLB. Then, when the room size is sufficiently large, the LOS-based VLP error will tend to its CRLB, and both are increasing with the room size. In this case, the scaling rate of the NLOS-based VLP error and LOS-based VLP error become the same.

6) The Impact of the Number of LEDs: The impact of $|\Theta_R|$ on the VLP performance is shown in Fig. 12, where $|\Theta_R|$ varies from 1 to 40 while the measurement noise strength is fixed at 10^{-8} (equivalent to an SNR around 30 dB for the case of 15 LEDs). We can see that the LOS-based VLP error will reduce and then tend to be saturated as $|\Theta_R|$ increases. This is due to the NLOS propagation-caused VLP error, which cannot be mitigated by deploying more LEDs. In contrast, the NLOS-based VLP error reduces with $|\Theta_R|$ at a rate of approximately $\mathcal{O}(|\Theta_R|^{-\frac{1}{2}})$ (for root mean squared error), which complies with Corollary 8. In addition, 10 LED arrays are sufficient for achieving satisfactory VLP performance. When $|\Theta_R| > 10$, the NLOS-based VLP performance gain from the increased LEDs will gradually become marginal due to the limited deployment area (room ceiling) of the LEDs.

[12]It should be noted that the strength of the NLOS component increases with the reduction of the NLOS path length, as shown in (16).

VII. Conclusion

In this paper, the performance limits of VLP methods in diffuse scattering environments are studied, where two typical VLP methods, i.e., the LOS-based and the NLOS-based VLP methods, are investigated.

Firstly, the closed-form error bounds of these two typical VLP methods are quantified to gain insights into the VLP performance limits under diffuse scattering effects. It is shown that the LOS-based VLP error is affected by both the noise and the NLOS component in RSS measurements, while the NLOS-based VLP error is determined by the measurement noise only. Hence, there will be an error floor in the LOS-based VLP method as the SNR increases, and the error floor depends on the NLOS signal strength, which has been quantified in the paper. In contrast, the NLOS-based VLP method has no such error floor as the SNR increases, since the propagation knowledge of NLOS signals is exploited in its UD localization.

Secondly, the effect of the NLOS propagation on the VLP performance limits is analyzed. To be specific, the performance gain of the NLOS-based VLP method (from harnessing the NLOS links) over the LOS-based VLP method is quantified. It is established that exploiting the NLOS propagation knowledge in UD localization can significantly improve the VLP performance, particularly in a high-SNR condition.

Appendix A
Proof of Theorem 1

We shall first derive the CRLB for the LOS-based estimate $\hat{\boldsymbol{\beta}}_{\text{UD}}^{\text{los}}$ for the joint vector $\boldsymbol{\beta}_{\text{UD}}^{\text{los}}$, and then we will derive the CRLBs for $\mathbf{x}$ and $\mathbf{u}$, separately. Let $\boldsymbol{\upsilon}$ be the bias of $\hat{\boldsymbol{\beta}}_{\text{UD}}^{\text{los}}$ due to the NLOS effect, i.e., $\boldsymbol{\upsilon} = \mathbb{E}\{\hat{\boldsymbol{\beta}}_{\text{UD}}^{\text{los}}\} - \boldsymbol{\beta}_{\text{UD}}$. Thus, the mean

squared error of $\hat{\boldsymbol{\beta}}_{\rm UD}^{\sf los}$ can be formulated as

$$\mathbb{E}\{\|\hat{\boldsymbol{\beta}}_{\rm UD}^{\sf los}-\boldsymbol{\beta}_{\rm UD}\|_2^2\}=\|\boldsymbol{\upsilon}\|_2^2+\underbrace{\mathbb{E}\{\|\hat{\boldsymbol{\beta}}_{\rm UD}^{\sf los}-\mathbb{E}\{\hat{\boldsymbol{\beta}}_{\rm UD}^{\sf los}\}\|_2^2\}}_{{\rm cov}(\hat{\boldsymbol{\beta}}_{\rm UD}^{\sf los})},$$

where it should be noted that $\mathbb{E}\{\|\boldsymbol{\upsilon}\|_2^2\}=\|\boldsymbol{\upsilon}\|_2^2$ and ${\rm cov}(\hat{\boldsymbol{\beta}}_{\rm UD}^{\sf los})$ is the covariance of estimate error, which follows [45],

$${\rm cov}(\hat{\boldsymbol{\beta}}_{\rm UD}^{\sf los})\geq{\rm trace}\big(\boldsymbol{\mathcal{B}}_{\boldsymbol{\beta}_{\rm UD}}^{\sf los}(\boldsymbol{\beta}_{\rm UD})\big),\tag{72}$$

$$\boldsymbol{\mathcal{B}}_{\boldsymbol{\beta}_{\rm UD}}^{\sf los}(\boldsymbol{\beta}_{\rm UD})=\big(\boldsymbol{\mathcal{I}}_{\boldsymbol{\beta}_{\rm UD}}^{\sf los}(\boldsymbol{\beta}_{\rm UD})\big)^{-1},\tag{73}$$

where $\boldsymbol{\mathcal{B}}_{\boldsymbol{\beta}_{\rm UD}}^{\sf los}(\boldsymbol{\beta}_{\rm UD})\in\mathbb{S}^6$ is the CRLB of joint variable $\boldsymbol{\beta}_{\rm UD}$, and $\boldsymbol{\mathcal{I}}_{\boldsymbol{\beta}_{\rm UD}}^{\sf los}(\boldsymbol{\beta}_{\rm UD})$ is the Fisher information matrix (FIM) [45],

$$\boldsymbol{\mathcal{I}}_{\boldsymbol{\beta}_{\rm UD}}^{\sf los}(\boldsymbol{\beta}_{\rm UD})=-\mathbb{E}_{\mathbf{z}|\boldsymbol{\beta}_{\rm UD}}\big\{\,\nabla_{\boldsymbol{\beta}_{\rm UD}}^2\ln p_{\sf los}\left(\mathbf{z}|\boldsymbol{\beta}_{\rm UD}\right)\big\},\tag{74}$$

where $\nabla_{\boldsymbol{\beta}_{\rm UD}}^2(\bullet)$ is the second-order derivative w.r.t. $\boldsymbol{\beta}_{\rm UD}$, and $p_{\sf los}(\mathbf{z}|\boldsymbol{\beta}_{\rm UD})=\mathcal{N}(\mathbf{z}|\mathbf{G}_{\sf los}(\mathbf{x})\boldsymbol{\mu}(\mathbf{u})+\boldsymbol{\varsigma}_{\sf nlos},\omega\mathbf{I}_{M_E|\Omega_R|})$ as per the system model, where $\boldsymbol{\mu}(\mathbf{u})=\dfrac{\mathbf{u}}{\|\mathbf{u}\|_2}$ and $\boldsymbol{\varsigma}_{\sf nlos}=\mathbf{G}_{\sf nlos}(\mathbf{x})\boldsymbol{\mu}(\mathbf{u})$ is the NLOS component.

Then, the FIM $\boldsymbol{\mathcal{I}}_{\boldsymbol{\beta}_{\rm UD}}^{\sf los}(\boldsymbol{\beta}_{\rm UD})$ will be eventually given by

$$\boldsymbol{\mathcal{I}}_{\boldsymbol{\beta}_{\rm UD}}^{\sf los}(\boldsymbol{\beta}_{\rm UD})=\begin{bmatrix}\boldsymbol{\mathcal{I}}_{\mathbf{x},\mathbf{x}}^{\sf los}(\mathbf{x},\mathbf{u}) & \boldsymbol{\mathcal{I}}_{\mathbf{x},\mathbf{u}}^{\sf los}(\mathbf{x},\mathbf{u})\\ \boldsymbol{\mathcal{I}}_{\mathbf{u},\mathbf{x}}^{\sf los}(\mathbf{x},\mathbf{u}) & \boldsymbol{\mathcal{I}}_{\mathbf{u},\mathbf{u}}^{\sf los}(\mathbf{x},\mathbf{u})\end{bmatrix},\tag{75}$$

where each 3×3 information element matrix is given by

$$\boldsymbol{\mathcal{I}}_{\mathbf{x},\mathbf{x}}^{\sf los}(\mathbf{x},\mathbf{u})=\omega\mathbf{H}_{\sf los}(\mathbf{x})\mathbf{U}(\mathbf{u})\mathbf{U}^\top(\mathbf{u})\mathbf{H}_{\sf los}^\top(\mathbf{x}),\tag{76}$$

$$\boldsymbol{\mathcal{I}}_{\mathbf{x},\mathbf{u}}^{\sf los}(\mathbf{x},\mathbf{u})=\omega\mathbf{H}_{\sf los}(\mathbf{x})\mathbf{U}(\mathbf{u})\mathbf{G}_{\sf los}(\mathbf{x})\boldsymbol{\mathcal{R}}^\top(\mathbf{u}),\tag{77}$$

$$\boldsymbol{\mathcal{I}}_{\mathbf{u},\mathbf{x}}^{\sf los}(\mathbf{x},\mathbf{u})=\boldsymbol{\mathcal{I}}_{\mathbf{x},\mathbf{u}}^{\top}(\mathbf{x},\mathbf{u}),\tag{78}$$

$$\boldsymbol{\mathcal{I}}_{\mathbf{u},\mathbf{u}}^{\sf los}(\mathbf{x},\mathbf{u})=\omega\boldsymbol{\mathcal{R}}(\mathbf{u})\mathbf{G}_{\sf los}^\top(\mathbf{x})\mathbf{G}_{\sf los}(\mathbf{x})\boldsymbol{\mathcal{R}}^\top(\mathbf{u}),\tag{79}$$

and $\mathbf{H}_{\sf los}(\mathbf{x})$, $\mathbf{U}(\mathbf{u})$, $\boldsymbol{\mathcal{R}}(\mathbf{u})$ and $\mathbf{G}_{\sf los}(\mathbf{x})$ is given by (27), (28), (30) and (19), respectively. Then, based on the structure of the joint variable $\boldsymbol{\beta}_{\rm UD}$'s CRLB and using Schur complement [43], the CRLB of $\mathbf{x}$ and $\mathbf{u}$ is eventually given by (25) and (26), respectively. Hence, Theorem 1 is proved.

APPENDIX B
PROOF OF THEOREM 2

For the LOS-based VLP method, only the LOS channel is exploited. Hence, its system model is recast as $\mathbf{z}=\mathbf{G}_{\sf los}(\mathbf{x})\boldsymbol{\mu}(\mathbf{u})+\boldsymbol{\varsigma}_{\sf nlos}+\boldsymbol{\epsilon}$, where $\boldsymbol{\varsigma}_{\sf nlos}=\mathbf{G}_{\sf nlos}(\mathbf{x})\boldsymbol{\mu}(\mathbf{u})$ is the NLOS component but is unknown for the LOS-based VLP. Let $\hat{\mathbf{z}}=\mathbf{G}_{\sf los}(\hat{\mathbf{x}}_{\sf los})\boldsymbol{\mu}(\hat{\mathbf{u}}_{\sf los})$ be the measurement guess of the LOS-based VLP method. Applying the first-order approximation around $\mathbf{x}=\mathbf{x}_{\sf true}$, where $\mathbf{x}_{\sf true}$ is the true value of $\mathbf{x}$, we obtain $\hat{\mathbf{z}}\approx\mathbf{G}_{\sf los}(\mathbf{x}_{\sf true})\boldsymbol{\mu}(\mathbf{u}_{\sf true})+\begin{bmatrix}\nabla_{\mathbf{x}}\big(\mathbf{G}_{\sf los}(\mathbf{x}_{\sf true})\boldsymbol{\mu}(\mathbf{u}_{\sf true})\big)\\ \nabla_{\mathbf{u}}\big(\mathbf{G}_{\sf los}(\mathbf{x}_{\sf true})\boldsymbol{\mu}(\mathbf{u}_{\sf true})\big)\end{bmatrix}^\top\begin{bmatrix}\hat{\mathbf{x}}_{\sf los}-\mathbf{x}_{\sf true}\\ \hat{\mathbf{u}}_{\sf los}-\mathbf{u}_{\sf true}\end{bmatrix}$ where the high-order infinitesimal error of $\mathcal{O}\big(\|\hat{\mathbf{x}}_{\sf los}-\mathbf{x}\|_2^2+\|\hat{\mathbf{u}}_{\sf los}-\mathbf{u}\|_2^2\big)$ is ignored. In addition, let $\boldsymbol{\varsigma}_{\sf resi}=\mathbf{z}-\hat{\mathbf{z}}$ be the residual measurement error of the LOS-based VLP, and let $\boldsymbol{\varsigma}_{\sf bias}=\boldsymbol{\varsigma}_{\sf nlos}-\boldsymbol{\varsigma}_{\sf resi}$. Since we know $\mathbf{z}=\mathbf{G}_{\sf los}(\mathbf{x}_{\sf true})\boldsymbol{\mu}(\mathbf{u}_{\sf true})+\boldsymbol{\varsigma}_{\sf nlos}+\boldsymbol{\epsilon}$ as per the system model, we have

$$\begin{bmatrix}\nabla_{\mathbf{x}}\big(\mathbf{G}_{\sf los}(\mathbf{x}_{\sf true})\boldsymbol{\mu}(\mathbf{u}_{\sf true})\big)\\ \nabla_{\mathbf{u}}\big(\mathbf{G}_{\sf los}(\mathbf{x}_{\sf true})\boldsymbol{\mu}(\mathbf{u}_{\sf true})\big)\end{bmatrix}^\top\begin{bmatrix}\hat{\mathbf{x}}_{\sf los}-\mathbf{x}_{\sf true}\\ \hat{\mathbf{u}}_{\sf los}-\mathbf{u}_{\sf true}\end{bmatrix}\approx\boldsymbol{\varsigma}_{\sf bias}+\boldsymbol{\epsilon}.\tag{80}$$

Then, taking the expectation of both sides of (80) over $\boldsymbol{\epsilon}$, we have $\begin{bmatrix}\nabla_{\mathbf{x}}\big(\mathbf{G}_{\sf los}(\mathbf{x}_{\sf true})\boldsymbol{\mu}(\mathbf{u}_{\sf true})\big)\\ \nabla_{\mathbf{u}}\big(\mathbf{G}_{\sf los}(\mathbf{x}_{\sf true})\boldsymbol{\mu}(\mathbf{u}_{\sf true})\big)\end{bmatrix}^\top\begin{bmatrix}\mathbb{E}\{\hat{\mathbf{x}}_{\sf los}\}-\mathbf{x}_{\sf true}\\ \mathbb{E}\{\hat{\mathbf{u}}_{\sf los}\}-\mathbf{u}_{\sf true}\end{bmatrix}\approx\boldsymbol{\varsigma}_{\sf bias}$, where we have assumed $\mathbb{E}\{\boldsymbol{\epsilon}\}=\mathbf{0}$. As a result, we arrive at (81), as shown at the bottom of this page. It should be noted that $\nabla_{\mathbf{x}}\big(\mathbf{G}_{\sf los}(\mathbf{x}_{\sf true})\boldsymbol{\mu}(\mathbf{u}_{\sf true})\big)=\mathbf{H}_{\sf los}(\mathbf{x})\mathbf{U}(\mathbf{u})$ and $\upsilon_{\mathbf{x}}=\|\mathbb{E}\{\hat{\mathbf{x}}_{\sf los}\}-\mathbf{x}_{\sf true}\|_2$. Hence, taking the trace of the 3×3 left-top submatrix and the 3×3 right-bottom submatrix of the correlation matrix $\boldsymbol{\varsigma}_{\sf bias}\boldsymbol{\varsigma}_{\sf bias}^\top$ in (81) and using the singular-value-decomposition of the left coefficient matrix, Theorem 2 is proved.

APPENDIX C
PROOF OF THEOREM 3

Let $\boldsymbol{\epsilon}_{\sf overall}=\boldsymbol{\varsigma}_{\sf bias}+\boldsymbol{\epsilon}$. Then, as per (80), we have (82), as shown at the bottom of the next page, and further have (83), as shown at the bottom of the next page. Hence, taking the trace of the 3×3 left-top submatrix and the 3×3 right-bottom submatrix of the left-hand-side correlation matrix in (83), the equations in Theorem 3 are obtained. An approximation with an error of $\mathcal{O}\big(\|\hat{\mathbf{x}}_{\sf los}-\mathbf{x}_{\sf true}\|_2^2+\|\hat{\mathbf{u}}_{\sf los}-\mathbf{u}_{\sf true}\|_2^2\big)$ is employed in (80), and hence the LOS-based VLP performance approximation error is $\mathcal{O}\big(\|\hat{\mathbf{x}}_{\sf los}-\mathbf{x}_{\sf true}\|_2^2+\|\hat{\mathbf{u}}_{\sf los}-\mathbf{u}_{\sf true}\|_2^2\big)$.

APPENDIX D
PROOF OF THEOREM 4

The derivation of the NLOS-based CRLBs follows from a similar idea to the LOS-based CRLBs in (25) and (26), where we only need to replay $\mathbf{G}_{\sf los}(\mathbf{x})$ by $\mathbf{G}(\mathbf{x})$. Hence, all FIMs should relate to the NLOS-based information. As per (74), the NLOS-based FIM $\boldsymbol{\mathcal{I}}_{\boldsymbol{\alpha}}(\boldsymbol{\beta}_{\rm UD})$ of joint variable $\boldsymbol{\alpha}$ follows

$$\boldsymbol{\mathcal{I}}_{\boldsymbol{\alpha}}(\boldsymbol{\beta}_{\rm UD})=\begin{bmatrix}\boldsymbol{\mathcal{I}}_{\mathbf{x},\mathbf{x}} & \boldsymbol{\mathcal{I}}_{\mathbf{x},\mathbf{u}} & \boldsymbol{\mathcal{I}}_{\mathbf{x},\mathbf{s}} & \boldsymbol{\mathcal{I}}_{\mathbf{x},\boldsymbol{\wp}}\\ \boldsymbol{\mathcal{I}}_{\mathbf{u},\mathbf{x}} & \boldsymbol{\mathcal{I}}_{\mathbf{u},\mathbf{u}} & \boldsymbol{\mathcal{I}}_{\mathbf{u},\mathbf{s}} & \boldsymbol{\mathcal{I}}_{\mathbf{u},\boldsymbol{\wp}}\\ \boldsymbol{\mathcal{I}}_{\mathbf{s},\mathbf{x}} & \boldsymbol{\mathcal{I}}_{\mathbf{s},\mathbf{u}} & \boldsymbol{\mathcal{I}}_{\mathbf{s},\mathbf{s}}^{\sf nlos} & \boldsymbol{\mathcal{I}}_{\mathbf{s},\boldsymbol{\wp}}^{\sf nlos}\\ \boldsymbol{\mathcal{I}}_{\boldsymbol{\wp},\mathbf{x}} & \boldsymbol{\mathcal{I}}_{\boldsymbol{\wp},\mathbf{u}} & \boldsymbol{\mathcal{I}}_{\boldsymbol{\wp},\mathbf{s}}^{\sf nlos} & \boldsymbol{\mathcal{I}}_{\boldsymbol{\wp},\boldsymbol{\wp}}^{\sf nlos}\end{bmatrix},\tag{84}$$

where each information element is given by

$$\boldsymbol{\mathcal{I}}_{\mathbf{x},\mathbf{x}}\in\mathbb{S}^3=\omega\mathbf{H}(\mathbf{x})\mathbf{U}(\mathbf{u})\mathbf{U}^\top(\mathbf{u})\mathbf{H}^\top(\mathbf{x}),\tag{85}$$

$$\boldsymbol{\mathcal{I}}_{\mathbf{x},\mathbf{u}}\in\mathbb{R}^{3\times3}=\omega\mathbf{H}(\mathbf{x})\mathbf{U}(\mathbf{u})\mathbf{G}(\mathbf{x})\boldsymbol{\mathcal{R}}^\top(\mathbf{u}),\tag{86}$$

$$\boldsymbol{\mathcal{I}}_{\mathbf{x},\mathbf{s}}\in\mathbb{R}^{3\times3L|\Omega_R|}=\omega\mathbf{H}(\mathbf{x})\mathbf{U}(\mathbf{u})\mathbf{U}^\top(\mathbf{u})\boldsymbol{\mathcal{H}}_{\sf nlos}^\top(\mathbf{x}),\tag{87}$$

$$\boldsymbol{\mathcal{I}}_{\mathbf{x},\boldsymbol{\wp}}\in\mathbb{R}^{3\times L|\Omega_R|}=\omega\mathbf{H}(\mathbf{x})\mathbf{U}(\mathbf{u})\mathbf{K}_{\sf nlos}(\mathbf{x},\mathbf{u}),\tag{88}$$

$$\boldsymbol{\mathcal{I}}_{\mathbf{u},\mathbf{u}}\in\mathbb{S}^3=\omega\boldsymbol{\mathcal{R}}(\mathbf{u})\mathbf{G}^\top(\mathbf{x})\mathbf{G}(\mathbf{x})\boldsymbol{\mathcal{R}}^\top(\mathbf{u}),\tag{89}$$

$$\boldsymbol{\mathcal{I}}_{\mathbf{u},\mathbf{s}}\in\mathbb{R}^{3\times3L|\Omega_R|}=\omega\boldsymbol{\mathcal{R}}(\mathbf{u})\mathbf{G}^\top(\mathbf{x})\mathbf{U}^\top(\mathbf{u})\boldsymbol{\mathcal{H}}_{\sf nlos}^\top(\mathbf{x}),\tag{90}$$

$$\boldsymbol{\mathcal{I}}_{\mathbf{u},\boldsymbol{\wp}}\in\mathbb{R}^{3\times L|\Omega_R|}=\omega\boldsymbol{\mathcal{R}}(\mathbf{u})\mathbf{G}^\top(\mathbf{x})\mathbf{K}_{\sf nlos}(\mathbf{x},\mathbf{u}),\tag{91}$$

$$\boldsymbol{\varsigma}_{\sf bias}\boldsymbol{\varsigma}_{\sf bias}^\top\approx\begin{bmatrix}\nabla_{\mathbf{x}}^\top\big(\mathbf{G}_{\sf los}(\mathbf{x}_{\sf true})\boldsymbol{\mu}(\mathbf{u}_{\sf true})\big)\\ \nabla_{\mathbf{u}}^\top\big(\mathbf{G}_{\sf los}(\mathbf{x}_{\sf true})\boldsymbol{\mu}(\mathbf{u}_{\sf true})\big)\end{bmatrix}\begin{bmatrix}\mathbb{E}\{\hat{\mathbf{x}}_{\sf los}\}-\mathbf{x}_{\sf true}\\ \mathbb{E}\{\hat{\mathbf{u}}_{\sf los}\}-\mathbf{u}_{\sf true}\end{bmatrix}\begin{bmatrix}\mathbb{E}\{\hat{\mathbf{x}}_{\sf los}\}-\mathbf{x}_{\sf true}\\ \mathbb{E}\{\hat{\mathbf{u}}_{\sf los}\}-\mathbf{u}_{\sf true}\end{bmatrix}^\top\begin{bmatrix}\nabla_{\mathbf{x}}\big(\mathbf{G}_{\sf los}(\mathbf{x}_{\sf true})\boldsymbol{\mu}(\mathbf{u}_{\sf true})\big)\\ \nabla_{\mathbf{u}}\big(\mathbf{G}_{\sf los}(\mathbf{x}_{\sf true})\boldsymbol{\mu}(\mathbf{u}_{\sf true})\big)\end{bmatrix}.\tag{81}$$

$$\boldsymbol{\mathcal{I}}^{\mathsf{nlos}}_{\mathbf{s},\mathbf{s}} \in \mathbb{S}^{3L|\Omega_R|} = \omega \boldsymbol{\mathcal{H}}_{\mathsf{nlos}}(\mathbf{x})\mathbf{U}(\mathbf{u})\mathbf{U}^{\top}(\mathbf{u})\boldsymbol{\mathcal{H}}^{\top}_{\mathsf{nlos}}(\mathbf{x}), \quad (92)$$

$$\boldsymbol{\mathcal{I}}^{\mathsf{nlos}}_{\mathbf{s},\boldsymbol{\wp}} \in \mathbb{R}^{3L|\Omega_R|\times L|\Omega_R|} = \omega \boldsymbol{\mathcal{H}}_{\mathsf{nlos}}(\mathbf{x})\mathbf{U}(\mathbf{u})\mathbf{K}_{\mathsf{nlos}}(\mathbf{x},\mathbf{u}), \quad (93)$$

$$\boldsymbol{\mathcal{I}}^{\mathsf{nlos}}_{\boldsymbol{\wp},\boldsymbol{\wp}} \in \mathbb{S}^{L|\Omega_R|} = \omega \mathbf{K}^{\top}_{\mathsf{nlos}}(\mathbf{x},\mathbf{u})\mathbf{K}_{\mathsf{nlos}}(\mathbf{x},\mathbf{u}), \quad (94)$$

where $\boldsymbol{\mathcal{H}}_{\mathsf{nlos}}(\mathbf{x}) \in \mathbb{R}^{3L|\Omega_R|\times 3M_E|\Omega_R|}$ is given by

$$\boldsymbol{\mathcal{H}}_{\mathsf{nlos}}(\mathbf{x}) = [\boldsymbol{\mathcal{H}}_{k,m} | \forall k = 1\!:\!M_E,\, \forall m \in \Omega_R], \quad (95)$$

$$\boldsymbol{\mathcal{H}}_{k,m} = \mathsf{mat}\,[\,\boldsymbol{\mathcal{H}}_{k,m;m'} | \forall m' \in \Omega_R], \quad (96)$$

in which $\boldsymbol{\mathcal{H}}_{k,m;m'} \in \mathbb{C}^{3L\times 3}$ is given by

$$\boldsymbol{\mathcal{H}}_{k,m;m'} = \begin{cases} \boldsymbol{\mathcal{H}}'_{k,m}, & \text{if } m' = m, \\ \mathbf{0}_{3L\times 3}, & \text{otherwise}, \end{cases} \quad (97)$$

$$\boldsymbol{\mathcal{H}}'_{k,m} = \mathsf{mat}\,[\,\boldsymbol{\mathcal{H}}'_{l,k,m} | \forall l = 1:L], \quad (98)$$

in which $\boldsymbol{\mathcal{H}}'_{l,k,m} \in \mathbb{R}^{3\times 3}$ is given by (99), as shown at the bottom of this page and $\varphi_{l,k,m} \in \mathbb{R}$ is given by (46). In addition, $\mathbf{K}_{\mathsf{nlos}}(\mathbf{x},\mathbf{u}) \in \mathbb{R}^{M_E|\Omega_R|\times L|\Omega_R|}$ is

$$\mathbf{K}_{\mathsf{nlos}}(\mathbf{x},\mathbf{u}) = \mathsf{diag}[\mathbf{K}_m(\mathbf{x},\mathbf{u}) | \forall m \in \Omega_R], \quad (100)$$

$$\mathbf{K}_m(\mathbf{x},\mathbf{u}) = \mathsf{mat}[\mathbf{q}^{\top}_{k,m}(\mathbf{x},\mathbf{u}) | \forall k = 1:M_E], \quad (101)$$

$$\mathbf{q}_{k,m}(\mathbf{x},\mathbf{u}) = \mathsf{vec}[q_{l,k,m} | \forall l = 1:L], \quad (102)$$

where $q_{l,k,m} \in \mathbb{R}$ is given by

$$q_{l,k,m} = \Psi_R \frac{(r+1)^2 \left((\mathbf{s}_{l,m} - \mathbf{p}_{k,m})^{\top}\mathbf{v}_{k,m}\right)^r (\mathbf{s}_{l,m} - \mathbf{x})^{\top}\mathbf{u}}{2\pi \|\mathbf{s}_{l,m} - \mathbf{p}_{k,m}\|_2^{r+2} \|\mathbf{x} - \mathbf{s}_{l,m}\|_2^3}.$$

Based on the structure of $\boldsymbol{\mathcal{I}}_{\boldsymbol{\alpha}}(\boldsymbol{\beta}_{\mathrm{UD}})$, applying Schur complement, the UD location-based FIM is given by

$$\boldsymbol{\mathcal{Q}}^{\mathsf{nlos}}_{\mathbf{x}}(\boldsymbol{\beta}_{\mathrm{UD}}) = \boldsymbol{\mathcal{I}}_{\mathbf{x},\mathbf{x}} - \boldsymbol{\mathcal{P}}_{\mathbf{x}}\mathbf{W}^{-1}_{\mathbf{x}}\boldsymbol{\mathcal{P}}^{\top}_{\mathbf{x}}, \quad (103)$$

$$= \omega \mathbf{H}(\mathbf{x})\mathbf{U}(\mathbf{u})\mathbf{U}^{\top}(\mathbf{u})\mathbf{H}^{\top}(\mathbf{x}) - \boldsymbol{\mathcal{P}}_{\mathbf{x}}\mathbf{W}^{-1}_{\mathbf{x}}\boldsymbol{\mathcal{P}}^{\top}_{\mathbf{x}}, \quad (104)$$

with $\boldsymbol{\mathcal{P}}_{\mathbf{x}} \in \mathbb{R}^{3\times(4L|\Omega_R|+3)}$ and $\mathbf{W}_{\mathbf{x}} \in \mathbb{S}^{(4L|\Omega_R|+3)}$ given by

$$\boldsymbol{\mathcal{P}}_{\mathbf{x}} = \begin{bmatrix} \boldsymbol{\mathcal{I}}_{\mathbf{x},\mathbf{u}} & \boldsymbol{\mathcal{I}}_{\mathbf{x},\mathbf{s}} & \boldsymbol{\mathcal{I}}_{\mathbf{x},\boldsymbol{\wp}} \end{bmatrix}, \quad (105)$$

$$\mathbf{W}_{\mathbf{x}} = \begin{bmatrix} \boldsymbol{\mathcal{I}}_{\mathbf{u},\mathbf{u}} & \boldsymbol{\mathcal{I}}_{\mathbf{u},\mathbf{s}} & \boldsymbol{\mathcal{I}}_{\mathbf{u},\boldsymbol{\wp}} \\ \boldsymbol{\mathcal{I}}_{\mathbf{s},\mathbf{u}} & \boldsymbol{\mathcal{I}}^{\mathsf{nlos}}_{\mathbf{s},\mathbf{s}} & \boldsymbol{\mathcal{I}}^{\mathsf{nlos}}_{\mathbf{s},\boldsymbol{\wp}} \\ \boldsymbol{\mathcal{I}}_{\boldsymbol{\wp},\mathbf{u}} & \boldsymbol{\mathcal{I}}^{\mathsf{nlos}}_{\boldsymbol{\wp},\mathbf{s}} & \boldsymbol{\mathcal{I}}^{\mathsf{nlos}}_{\boldsymbol{\wp},\boldsymbol{\wp}} \end{bmatrix}, \quad (106)$$

and each element $\boldsymbol{\mathcal{I}}_{\bullet,\bullet}$ has been given by (85)–(94).

Rearranging $\boldsymbol{\mathcal{I}}_{\boldsymbol{\alpha}}(\boldsymbol{\beta}_{\mathrm{UD}})$ and applying the Schur complement, the UD orientation-based FIM $\boldsymbol{\mathcal{Q}}^{\mathsf{nlos}}_{\mathbf{u}}(\boldsymbol{\beta}_{\mathrm{UD}})$ is given by

$$\boldsymbol{\mathcal{Q}}^{\mathsf{nlos}}_{\mathbf{u}}(\boldsymbol{\beta}_{\mathrm{UD}}) = \boldsymbol{\mathcal{I}}_{\mathbf{u},\mathbf{u}} - \boldsymbol{\mathcal{P}}_{\mathbf{u}}\mathbf{W}^{-1}_{\mathbf{u}}\boldsymbol{\mathcal{P}}^{\top}_{\mathbf{u}}, \quad (107)$$

$$= \boldsymbol{\mathcal{R}}(\mathbf{u})\mathbf{G}^{\top}(\mathbf{x})\mathbf{G}(\mathbf{x})\boldsymbol{\mathcal{R}}^{\top}(\mathbf{u}) - \boldsymbol{\mathcal{P}}_{\mathbf{u}}\mathbf{W}^{-1}_{\mathbf{u}}\boldsymbol{\mathcal{P}}^{\top}_{\mathbf{u}}, \quad (108)$$

with $\boldsymbol{\mathcal{P}}_{\mathbf{u}} \in \mathbb{R}^{3\times(4L|\Omega_R|+3)}$ and $\mathbf{W}_{\mathbf{u}} \in \mathbb{S}^{(4L|\Omega_R|+3)}$ given by

$$\boldsymbol{\mathcal{P}}_{\mathbf{u}} = \begin{bmatrix} \boldsymbol{\mathcal{I}}_{\mathbf{u},\mathbf{x}} & \boldsymbol{\mathcal{I}}_{\mathbf{u},\mathbf{s}} & \boldsymbol{\mathcal{I}}_{\mathbf{u},\boldsymbol{\wp}} \end{bmatrix}, \quad (109)$$

$$\mathbf{W}_{\mathbf{u}} = \begin{bmatrix} \boldsymbol{\mathcal{I}}_{\mathbf{x},\mathbf{x}} & \boldsymbol{\mathcal{I}}_{\mathbf{x},\mathbf{s}} & \boldsymbol{\mathcal{I}}_{\mathbf{x},\boldsymbol{\wp}} \\ \boldsymbol{\mathcal{I}}_{\mathbf{s},\mathbf{x}} & \boldsymbol{\mathcal{I}}^{\mathsf{nlos}}_{\mathbf{s},\mathbf{s}} & \boldsymbol{\mathcal{I}}^{\mathsf{nlos}}_{\mathbf{s},\boldsymbol{\wp}} \\ \boldsymbol{\mathcal{I}}_{\boldsymbol{\wp},\mathbf{x}} & \boldsymbol{\mathcal{I}}^{\mathsf{nlos}}_{\boldsymbol{\wp},\mathbf{s}} & \boldsymbol{\mathcal{I}}^{\mathsf{nlos}}_{\boldsymbol{\wp},\boldsymbol{\wp}} \end{bmatrix}. \quad (110)$$

As per (104) and (108), we have $\boldsymbol{\mathfrak{B}}^{\mathsf{nlos}}_{\mathbf{x}} = \left(\boldsymbol{\mathcal{Q}}^{\mathsf{nlos}}_{\mathbf{x}}(\boldsymbol{\beta}_{\mathrm{UD}})\right)^{-1}$ and $\boldsymbol{\mathfrak{B}}^{\mathsf{nlos}}_{\mathbf{u}} = \left(\boldsymbol{\mathcal{Q}}^{\mathsf{nlos}}_{\mathbf{u}}(\boldsymbol{\beta}_{\mathrm{UD}})\right)^{-1}$. As per the estimation theory, the UD location and orientation errors will be bounded by the respective CRLB, as shown in (39) and (40).

Appendix E
Proof of Lemma 1

As per (83) in Appendix C, the LOS-based localization error covariance matrix follows that

$$\mathbb{E}\{(\hat{\mathbf{x}}_{\mathsf{los}} - \mathbf{x})(\hat{\mathbf{x}}_{\mathsf{los}} - \mathbf{x})^{\top}\} \approx \boldsymbol{\mathfrak{B}}^{\mathsf{los}}_{\mathbf{x}} + \boldsymbol{\mathfrak{B}}^{\mathsf{bias}}_{\mathbf{x}}, \quad (111)$$

where $\boldsymbol{\mathfrak{B}}^{\mathsf{bias}}_{\mathbf{x}} = \|\boldsymbol{\varsigma}_{\mathsf{bias}}\|_2^2 \left(\mathbf{H}_{\mathsf{los}}(\mathbf{x})\mathbf{U}(\mathbf{u})\mathbf{U}^{\top}(\mathbf{u})\,\mathbf{H}^{\top}_{\mathsf{los}}(\mathbf{x})\right)^{-1}$.

Then, given $\boldsymbol{\mathcal{J}}^{\mathsf{bias}}_{\mathbf{x}}$ defined in (52) and taking the inverse of both sides of (111), the LOS-based VLP information $\tilde{\boldsymbol{\mathcal{Q}}}^{\mathsf{los}}_{\mathbf{x}}$ can be approximated by the equivalent FIM $\boldsymbol{\mathcal{Q}}^{\mathsf{los}}_{\mathbf{x}}$ given in (53).

$$\mathbb{E}\{\boldsymbol{\epsilon}_{\mathsf{overall}}\boldsymbol{\epsilon}^{\top}_{\mathsf{overall}}\} \approx \mathbb{E}\left\{ \begin{bmatrix} \nabla^{\top}_{\mathbf{x}}\left(\mathbf{G}_{\mathsf{los}}(\mathbf{x}_{\mathsf{true}})\boldsymbol{\mu}(\mathbf{u}_{\mathsf{true}})\right) \\ \nabla^{\top}_{\mathbf{u}}\left(\mathbf{G}_{\mathsf{los}}(\mathbf{x}_{\mathsf{true}})\boldsymbol{\mu}(\mathbf{u}_{\mathsf{true}})\right) \end{bmatrix} \begin{bmatrix} \hat{\mathbf{x}}_{\mathsf{los}} - \mathbf{x}_{\mathsf{true}} \\ \hat{\mathbf{u}}_{\mathsf{los}} - \mathbf{u}_{\mathsf{true}} \end{bmatrix} \begin{bmatrix} \hat{\mathbf{x}}_{\mathsf{los}} - \mathbf{x}_{\mathsf{true}} \\ \hat{\mathbf{u}}_{\mathsf{los}} - \mathbf{u}_{\mathsf{true}} \end{bmatrix}^{\top} \begin{bmatrix} \nabla_{\mathbf{x}}\left(\mathbf{G}_{\mathsf{los}}(\mathbf{x}_{\mathsf{true}})\boldsymbol{\mu}(\mathbf{u}_{\mathsf{true}})\right) \\ \nabla_{\mathbf{u}}\left(\mathbf{G}_{\mathsf{los}}(\mathbf{x}_{\mathsf{true}})\boldsymbol{\mu}(\mathbf{u}_{\mathsf{true}})\right) \end{bmatrix} \right\}. \quad (82)$$

$$\mathbb{E}\left\{ \begin{bmatrix} \hat{\mathbf{x}}_{\mathsf{los}} - \mathbf{x}_{\mathsf{true}} \\ \hat{\mathbf{u}}_{\mathsf{los}} - \mathbf{u}_{\mathsf{true}} \end{bmatrix} \begin{bmatrix} \hat{\mathbf{x}}_{\mathsf{los}} - \mathbf{x}_{\mathsf{true}} \\ \hat{\mathbf{u}}_{\mathsf{los}} - \mathbf{u}_{\mathsf{true}} \end{bmatrix}^{\top} \right\} \approx \begin{bmatrix} \mathbf{U}^{\top}(\mathbf{u}_{\mathsf{true}})\mathbf{H}^{\top}_{\mathsf{los}}(\mathbf{x}_{\mathsf{true}}) \\ \boldsymbol{\mathcal{R}}(\mathbf{u}_{\mathsf{true}})\mathbf{G}^{\top}_{\mathsf{los}}(\mathbf{x}_{\mathsf{true}}) \end{bmatrix}^{\dagger} \mathbb{E}\{\boldsymbol{\varsigma}_{\mathsf{bias}}\boldsymbol{\varsigma}^{\top}_{\mathsf{bias}}\} \begin{bmatrix} \mathbf{H}_{\mathsf{los}}(\mathbf{x}_{\mathsf{true}})\mathbf{U}(\mathbf{u}_{\mathsf{true}}) \\ \mathbf{G}_{\mathsf{los}}(\mathbf{x}_{\mathsf{true}})\boldsymbol{\mathcal{R}}^{\top}(\mathbf{u}_{\mathsf{true}}) \end{bmatrix}^{\dagger}$$
$$+ \underbrace{\begin{bmatrix} \mathbf{U}^{\top}(\mathbf{u}_{\mathsf{true}})\mathbf{H}^{\top}_{\mathsf{los}}(\mathbf{x}_{\mathsf{true}}) \\ \mathbf{G}_{\mathsf{los}}(\mathbf{x}_{\mathsf{true}})\boldsymbol{\mathcal{R}}^{\top}(\mathbf{u}_{\mathsf{true}}) \end{bmatrix}^{\dagger} \mathbb{E}\{\boldsymbol{\epsilon}\boldsymbol{\epsilon}^{\top}\} \begin{bmatrix} \mathbf{H}_{\mathsf{los}}(\mathbf{x}_{\mathsf{true}})\mathbf{U}(\mathbf{u}_{\mathsf{true}}) \\ \boldsymbol{\mathcal{R}}(\mathbf{u}_{\mathsf{true}})\mathbf{G}^{\top}_{\mathsf{los}}(\mathbf{x}_{\mathsf{true}}) \end{bmatrix}^{\dagger}}_{\text{LOS-based CRLB}}. \quad (83)$$

$$\boldsymbol{\mathcal{H}}'_{l,k,m} = \Psi_R \frac{r(r+1)^2}{2\pi} \frac{\wp_{l,m}\left((\mathbf{s}_{l,m} - \mathbf{p}_{k,m})^{\top}\mathbf{v}_{k,m}\right)^{r-1}}{\|\mathbf{s}_{l,m} - \mathbf{p}_{k,m}\|_2^{r+2}\|\mathbf{s}_{l,m} - \mathbf{x}\|_2^3} \mathbf{v}_{k,m}(\mathbf{s}_{l,m} - \mathbf{x})^{\top}$$
$$- \Psi_R \frac{(r+2)(r+1)^2}{2\pi} \frac{\wp_{l,m}\varphi_{l,k,m}}{\|\mathbf{s}_{l,m} - \mathbf{p}_{k,m}\|_2^2\|\mathbf{s}_{l,m} - \mathbf{x}\|_2^3} (\mathbf{s}_{l,m} - \mathbf{p}_m)(\mathbf{s}_{l,m} - \mathbf{x})^{\top}$$
$$+ \Psi_R \frac{(r+1)^2}{2\pi} \frac{\wp_{l,m}\varphi_{l,k,m}}{\|\mathbf{x} - \mathbf{s}_{l,m}\|_2^3} \mathbf{I}_3 - \Psi_R \frac{3(r+1)^2}{4\pi^2} \frac{\wp_{l,m}\varphi_{l,k,m}}{\|\mathbf{x} - \mathbf{s}_{l,m}\|_2^5} (\mathbf{s}_{l,m} - \mathbf{x})(\mathbf{s}_{l,m} - \mathbf{x})^{\top}. \quad (99)$$

$$\begin{aligned}\boldsymbol{\mathcal{J}}_{\mathbf{x}}(\boldsymbol{\beta}_{\mathrm{UD}}) &= \underbrace{\omega\mathbf{H}_{\mathsf{los}}(\mathbf{x})\mathbf{U}(\mathbf{u})\mathbf{U}^{\top}(\mathbf{u})\mathbf{H}_{\mathsf{los}}^{\top}(\mathbf{x}) - \omega\mathbf{H}_{\mathsf{los}}(\mathbf{x})\mathbf{U}(\mathbf{u})\mathbf{F}_{\mathsf{los}}^{\perp}(\mathbf{x})\mathbf{U}^{\top}(\mathbf{u})\mathbf{H}_{\mathsf{los}}^{\top}(\mathbf{x})}_{\boldsymbol{\mathcal{J}}_{\mathbf{x}}^{\mathsf{los}}(\mathbf{x},\mathbf{u})} \\ &\quad + \underbrace{\omega\mathbf{H}_{\mathsf{los}}(\mathbf{x})\mathbf{U}(\mathbf{u})\mathbf{U}^{\top}(\mathbf{u})\mathbf{H}_{\mathsf{nlos}}^{\top}(\mathbf{x}) + \omega\mathbf{H}_{\mathsf{nlos}}(\mathbf{x})\mathbf{U}(\mathbf{u})\mathbf{U}^{\top}(\mathbf{u})\big(\mathbf{H}_{\mathsf{los}}^{\top}(\mathbf{x}) + \mathbf{H}_{\mathsf{nlos}}^{\top}(\mathbf{x})\big)}_{\boldsymbol{\mathcal{D}}_{\mathbf{x}}^{\mathsf{nlos}}(\mathbf{x},\mathbf{u})} \\ &\quad - \underbrace{\big(\boldsymbol{\mathcal{P}}_{\mathbf{x}}\mathbf{W}_{\mathbf{x}}\boldsymbol{\mathcal{P}}_{\mathbf{x}}^{\top} - \omega\mathbf{H}_{\mathsf{los}}(\mathbf{x})\mathbf{U}(\mathbf{u})\mathbf{F}_{\mathsf{los}}^{\perp}(\mathbf{x})\mathbf{U}^{\top}(\mathbf{u})\mathbf{H}_{\mathsf{los}}^{\top}(\mathbf{x})\big)}_{\boldsymbol{\mathcal{S}}_{\mathbf{x}}^{\mathsf{nlos}}(\mathbf{x},\mathbf{u})}. \end{aligned} \tag{112}$$

APPENDIX F
PROOF OF COROLLARY 3

Based on the definition, we have $\boldsymbol{\mathcal{W}}_{\mathbf{x}}^{\mathsf{los}} = \boldsymbol{\mathcal{J}}_{\mathbf{x}}^{\mathsf{los}} - \boldsymbol{\mathcal{Q}}_{\mathbf{x}}^{\mathsf{los}} = \boldsymbol{\mathcal{J}}_{\mathbf{x}}^{\mathsf{los}} - \big(\big(\boldsymbol{\mathcal{J}}_{\mathbf{x}}^{\mathsf{los}}\big)^{-1} + \big(\boldsymbol{\mathcal{J}}_{\mathbf{x}}^{\mathsf{bias}}\big)^{-1}\big)^{-1}$. Then, applying for the inverse matrix lemma [43], [44], we finally arrive at (54). Thus, Corollary 3 is proved.

APPENDIX G
PROOF OF COROLLARY 4

We know $\mathbf{H}(\mathbf{x}) = \mathbf{H}_{\mathsf{los}}(\mathbf{x}) + \mathbf{H}_{\mathsf{nlos}}(\mathbf{x})$, where $\mathbf{H}_{\mathsf{nlos}}(\mathbf{x})$ is gvien by (58), and hence $\boldsymbol{\mathcal{I}}_{\mathbf{x},\mathbf{x}}$ in (85) can also be cast as

$$\boldsymbol{\mathcal{I}}_{\mathbf{x},\mathbf{x}} = \omega\big(\mathbf{H}_{\mathsf{los}}(\mathbf{x}) + \mathbf{H}_{\mathsf{nlos}}(\mathbf{x})\big)\mathbf{U}(\mathbf{u})\mathbf{U}^{\top}(\mathbf{u})\big(\mathbf{H}_{\mathsf{los}}^{\top}(\mathbf{x}) + \mathbf{H}_{\mathsf{nlos}}^{\top}(\mathbf{x})\big).$$

Therefore, $\boldsymbol{\mathcal{J}}_{\mathbf{x}}(\boldsymbol{\beta}_{\mathrm{UD}})$ follows (112), as shown at the top of this page. Hence, combining (112) with (55), the NLOS-based information $\boldsymbol{\mathcal{J}}_{\mathbf{x}}^{\mathsf{nlos}}(\mathbf{x},\mathbf{u})$ in (56) is obtained. Hence, Corollary 4 is proved.

APPENDIX H
PROOF OF COROLLARY 7

Based on (85), (43), (44), (45) and (31), we know that $\boldsymbol{\mathcal{I}}_{\mathbf{x},\mathbf{x}}$ is $\mathcal{O}(\rho_{\min}^{-6})$, as $\rho_{\min} \to \infty$. We can observe from (105), (106) and (86)–(94) that $\boldsymbol{\mathcal{P}}_{\mathbf{x}}\mathbf{W}_{\mathbf{x}}^{-1}\boldsymbol{\mathcal{P}}_{\mathbf{x}}^{\top}$ is $\mathcal{O}(\rho_{\min}^{-6})$. Hence, based on (103), we know $\boldsymbol{\mathcal{Q}}_{\mathbf{x}}^{\mathsf{nlos}}$ is $\mathcal{O}(\rho_{\min}^{-6})$. Thus, (64) is obtained. In the same way, based on (89), (18), (19), (20), (15) and (16), we have $\boldsymbol{\mathcal{I}}_{\mathbf{u},\mathbf{u}} \sim \mathcal{O}(\rho_{\min}^{-4})$. Based on (109), (110) and (85)–(94), we know $\boldsymbol{\mathcal{P}}_{\mathbf{u}}\mathbf{W}_{\mathbf{u}}^{-1}\boldsymbol{\mathcal{P}}_{\mathbf{u}}^{\top}$ is $\mathcal{O}(\rho_{\min}^{-4})$. Hence, as per (107), we know $\boldsymbol{\mathcal{Q}}_{\mathbf{u}}^{\mathsf{nlos}}$ follows $\mathcal{O}(\rho_{\min}^{-4})$. Thus, (65) is obtained.

APPENDIX I
PROOF OF COROLLARY 8

Let us first consider the error bound $\mathfrak{B}_{\boldsymbol{\alpha}}(\boldsymbol{\beta}_{\mathrm{UD}})$ of the joint variable $\boldsymbol{\alpha} = [\mathbf{x}, \mathbf{u}, \mathbf{s}, \wp]$, whose FIM $\boldsymbol{\mathcal{I}}_{\boldsymbol{\alpha}}(\boldsymbol{\beta}_{\mathrm{UD}})$ is given in (84)–(94). It can be easily verified that all information elements in $\boldsymbol{\mathcal{I}}_{\boldsymbol{\alpha}}(\boldsymbol{\beta}_{\mathrm{UD}})$ are $\Theta(|\Omega_R|)$. For instance, as shown in (85) and (43), the FIM element $\boldsymbol{\mathcal{I}}_{\mathbf{x},\mathbf{x}}$ follows that

$$\mathbf{H}(\mathbf{x})\mathbf{U}(\mathbf{u})\mathbf{U}^{\top}(\mathbf{u})\mathbf{H}^{\top}(\mathbf{x}) = \sum_{m\in\Omega_R}\mathbf{H}_m(\mathbf{x})\boldsymbol{\mu}(\mathbf{u})\boldsymbol{\mu}^{\top}(\mathbf{u})\mathbf{H}_m^{\top}(\mathbf{x}),$$

where $\mathbf{H}_m(\mathbf{x})$ is the mth component of $\mathbf{H}(\mathbf{x})$. Hence, if the LEDs are uniformly distributed, we have $\boldsymbol{\mathcal{I}}_{\boldsymbol{\alpha}}(\boldsymbol{\beta}_{\mathrm{UD}}) \sim \Theta(|\Omega_R|)$, and thus $\mathfrak{B}_{\boldsymbol{\alpha}}(\boldsymbol{\beta}_{\mathrm{UD}}) \sim \Theta(|\Omega_R|^{-1})$ as $\mathfrak{B}_{\boldsymbol{\alpha}}(\boldsymbol{\beta}_{\mathrm{UD}}) = (\boldsymbol{\mathcal{I}}_{\boldsymbol{\alpha}}(\boldsymbol{\beta}_{\mathrm{UD}}))^{-1}$. Since $\mathfrak{B}_{\mathbf{x}}^{\mathsf{nlos}}(\mathbf{x},\mathbf{u})$ and $\mathfrak{B}_{\mathbf{u}}^{\mathsf{nlos}}(\mathbf{x},\mathbf{u})$ is the top-left and right-bottom 3×3 submatrix, respectively, of $\mathfrak{B}_{\boldsymbol{\alpha}}(\boldsymbol{\beta}_{\mathrm{UD}})$, both are $\Theta(|\Omega_R|^{-1})$. Thus, Corollary 8 is proved.

APPENDIX J
PROOF OF COROLLARIES 9 AND 10

Firstly, we give the proof of Corollary 9. For the NLOS-based VLP method, as $\|\wp\|_2 \to \infty$, based on (57) we have $\boldsymbol{\mathcal{D}}_{\mathbf{x}}^{\mathsf{nlos}}(\mathbf{x},\mathbf{u}) \sim \mathcal{O}(\|\wp\|_2^2)$. Similarly, $\boldsymbol{\mathcal{S}}_{\mathbf{x}}^{\mathsf{nlos}} \sim \mathcal{O}(\|\wp\|_2^2)$. Hence, based on (56), we know $\boldsymbol{\mathcal{J}}_{\mathbf{x}}^{\mathsf{nlos}}(\mathbf{x},\mathbf{u}) \sim \mathcal{O}(\|\wp\|_2^2)$. Thus, (68) is obtained, and so is (69).

Secondly, we give the proof of Corollary 10. For the LOS-based VLP method, as $\|\wp\|_2 \to \infty$, $\|\varsigma_{\mathsf{nlos}}\|_2^2 \sim \mathcal{O}(\|\wp\|_2^2)$, and hence based on (52) we have $\boldsymbol{\mathcal{J}}_{\mathbf{x}}^{\mathsf{bias}}(\mathbf{x},\mathbf{u}) \sim \mathcal{O}(\|\wp\|_2^{-2})$. Thus, (70) is obtained, and so is (71).

REFERENCES

[1] E. Cardarelli, V. Digani, L. Sabattini, C. Secchi, and C. Fantuzzi, "Cooperative cloud robotics architecture for the coordination of multi-AGV systems in industrial warehouses," *Mechatronics*, vol. 45, pp. 1–13, Aug. 2017.

[2] R. Krug *et al.*, "The next step in robot commissioning: Autonomous picking and palletizing," *IEEE Robot. Autom. Lett.*, vol. 1, no. 1, pp. 546–553, Jan. 2016.

[3] J. Moon, I. Bae, and S. Kim, "Real-time near-optimal path and maneuver planning in automatic parking using a simultaneous dynamic optimization approach," in *Proc. IEEE Intell. Vehicles Symp. (IV)*, Jun. 2017, pp. 193–196.

[4] J. Armstrong, Y. Sekercioglu, and A. Neild, "Visible light positioning: A roadmap for international standardization," *IEEE Commun. Mag.*, vol. 51, no. 12, pp. 68–73, Dec. 2013.

[5] L. Yin, X. Wu, and H. Haas, "Indoor visible light positioning with angle diversity transmitter," in *Proc. IEEE 82nd Veh. Technol. Conf. (VTC-Fall)*, Sep. 2015, pp. 1–5.

[6] G. B. Prince and T. D. C. Little, "Latency constrained device positioning using a visible light communication two-phase received signal strength–angle of arrival algorithm," in *Proc. Int. Conf. Indoor Positioning Indoor Navigat. (IPIN)*, Oct. 2015, pp. 1–7.

[7] H.-S. Kim, D.-R. Kim, S.-H. Yang, Y.-H. Son, and S.-K. Han, "An indoor visible light communication positioning system using a RF carrier allocation technique," *J. Lightw. Technol.*, vol. 31, no. 1, pp. 134–144, Jan. 1, 2013.

[8] C. Sertthin, T. Ohtsuki, and M. Nakagawa, "6-axis sensor assisted low complexity high accuracy-visible light communication based indoor positioning system," *IEICE Trans. Commun.*, vol. E93-B, no. 11, pp. 2879–2891, 2010.

[9] Y. S. Eroglu, I. Guvenc, N. Pala, and M. Yuksel, "AOA-based localization and tracking in multi-element VLC systems," in *Proc. IEEE 16th Annu. Wireless Microw. Technol. Conf. (WAMICON)*, Cocoa Beach, FL, USA, Apr. 2015, pp. 1–5.

[10] H. Sharifi, A. Kumar, F. Alam, and K. M. Arif, "Indoor localization of mobile robot with visible light communication," in *Proc. 12th IEEE/ASME Int. Conf. Mech. Embedded Syst. Appl. (MESA)*, Aug. 2016, pp. 1–6.

[11] W. Zhang, M. I. S. Chowdhury, and M. Kavehrad, "Asynchronous indoor positioning system based on visible light communications," *Opt. Eng.*, vol. 53, no. 4, Apr. 2014, Art. no. 045105.

[12] A. Sahin, Y. S. Eroglu, I. Guvenc, N. Pala, and M. Yuksel, "Accuracy of AOA-based and RSS-based 3D localization for visible light communications," in *Proc. IEEE 82nd Veh. Technol. Conf. (VTC-Fall)*, Sep. 2015, pp. 1–5.

[13] B. Zhou, V. Lau, Q. Chen, and Y. Cao, "Simultaneous positioning and orientating for visible light communications: Algorithm design and performance analysis," *IEEE Trans. Veh. Technol.*, vol. 67, no. 12, pp. 11790–11804, Dec. 2018.

[14] X. Zhang, J. Duan, Y. Fu, and A. Shi, "Theoretical accuracy analysis of indoor visible light communication positioning system based on received signal strength indicator," *J. Lightw. Technol.*, vol. 32, no. 21, pp. 4180–4186, Nov. 1, 2014.

[15] Y. Zhuang, Q. Wang, M. Shi, P. Cao, L. Qi, and J. Yang, "Low-power centimeter-level localization for indoor mobile robots based on ensemble Kalman smoother using received signal strength," *IEEE Internet Things J.*, vol. 6, no. 4, pp. 6513–6522, Aug. 2019.

[16] B. Zhou, A. Liu, and V. Lau, "Robust visible light-based positioning under unknown user device orientation angle," in *Proc. 12th Int. Conf. Signal Process. Commun. Syst. (ICSPCS)*, Dec. 2018, pp. 1–5.

[17] B. Zhou, A. Liu, and V. Lau, "Joint user location and orientation estimation for visible light communication systems with unknown power emission," *IEEE Trans. Wireless Commun.*, vol. 18, no. 11, pp. 5181–5195, Nov. 2019.

[18] Z. Zhou, "Indoor positioning algorithm using light-emitting diode visible light communications," *Opt. Eng.*, vol. 51, no. 8, Aug. 2012, Art. no. 085009.

[19] S.-H. Yang, H.-S. Kim, Y.-H. Son, and S.-K. Han, "Three-dimensional visible light indoor localization using AOA and RSS with multiple optical receivers," *J. Lightw. Technol.*, vol. 32, no. 14, pp. 2480–2485, Jul. 1, 2014.

[20] Y. Zhuang *et al.*, "A survey of positioning systems using visible LED lights," *IEEE Commun. Surveys Tuts.*, vol. 20, no. 3, pp. 1963–1988, 3rd Quart., 2018.

[21] A. Al-Kinani, J. Sun, C.-X. Wang, W. Zhang, X. Ge, and H. Haas, "A 2-D non-stationary GBSM for vehicular visible light communication channels," *IEEE Trans. Wireless Commun.*, vol. 17, no. 12, pp. 7981–7992, Dec. 2018.

[22] B. Zhou, A. Liu, and V. Lau, "Performance limits of visible light-based user position and orientation estimation using received signal strength under NLOS propagation," *IEEE Trans. Wireless Commun.*, vol. 18, no. 11, pp. 5227–5241, Nov. 2019.

[23] C. Amini, A. Taherpour, T. Khattab, and S. Gazor, "Theoretical accuracy analysis of indoor visible light communication positioning system based on time-of-arrival," in *Proc. IEEE Can. Conf. Electr. Comput. Eng. (CCECE)*, Vancouver, BC, Canada, May 2016, pp. 1–5.

[24] H. Steendam, T. Q. Wang, and J. Armstrong, "Cramer-rao bound for indoor visible light positioning using an aperture-based angular-diversity receiver," in *Proc. IEEE Int. Conf. Commun. (ICC)*, Kuala Lumpur, Malaysia, May 2016, pp. 1–6.

[25] T. Q. Wang, Y. A. Sekercioglu, A. Neild, and J. Armstrong, "Position accuracy of time-of-arrival based ranging using visible light with application in indoor localization systems," *J. Lightw. Technol.*, vol. 31, no. 20, pp. 3302–3308, Oct. 15, 2013.

[26] A. Sahin, Y. S. Eroglu, I. Guvenc, N. Pala, and M. Yuksel, "Hybrid 3-D localization for visible light communication systems," *J. Lightw. Technol.*, vol. 33, no. 22, pp. 4589–4599, Nov. 15, 2015.

[27] Y. S. Eroglu, I. Guvenc, A. Sahin, Y. Yapici, N. Pala, and M. Yuksel, "Multi-element VLC networks: LED assignment, power control, and optimum combining," *IEEE J. Sel. Areas Commun.*, vol. 36, no. 1, pp. 121–135, Jan. 2018.

[28] Z. Chen, D. A. Basnayaka, and H. Haas, "Space division multiple access for optical attocell network using angle diversity transmitters," *J. Lightw. Technol.*, vol. 35, no. 11, pp. 2118–2131, Jun. 1, 2017.

[29] L. Zeng *et al.*, "High data rate multiple input multiple output (MIMO) optical wireless communications using white led lighting," *IEEE J. Sel. Areas Commun.*, vol. 27, no. 9, pp. 1654–1662, Dec. 2009.

[30] J. R. Barry, J. M. Kahn, W. J. Krause, E. A. Lee, and D. G. Messerschmitt, "Simulation of multipath impulse response for indoor wireless optical channels," *IEEE J. Sel. Areas Commun.*, vol. 11, no. 3, pp. 367–379, Apr. 1993.

[31] P. Luo, Z. Ghassemlooy, H. Le Minh, E. Bentley, A. Burton, and X. Tang, "Fundamental analysis of a car to car visible light communication system," in *Proc. 9th Int. Symp. Commun. Syst., Netw. Digit. Sign (CSNDSP)*, Jul. 2014, pp. 1011–1016.

[32] A. Liu, V. Lau, and W. Dai, "Joint burst LASSO for sparse channel estimation in multi-user massive MIMO," in *Proc. IEEE Int. Conf. Commun. (ICC)*, May 2016, pp. 1–6.

[33] X. Gao, O. Edfors, F. Rusek, and F. Tufvesson, "Linear pre-coding performance in measured very-large MIMO channels," in *Proc. IEEE Veh. Technol. Conf. (VTC Fall)*, Sep. 2011, pp. 1–5.

[34] C. R. Berger, Z. Wang, J. Huang, and S. Zhou, "Application of compressive sensing to sparse channel estimation," *IEEE Commun. Mag.*, vol. 48, no. 11, pp. 164–174, Nov. 2010.

[35] W. U. Bajwa, J. Haupt, A. M. Sayeed, and R. Nowak, "Compressed channel sensing: A new approach to estimating sparse multipath channels," *Proc. IEEE*, vol. 98, no. 6, pp. 1058–1076, Jun. 2010.

[36] Y. Barbotin, A. Hormati, S. Rangan, and M. Vetterli, "Estimation of sparse MIMO channels with common support," *IEEE Trans. Commun.*, vol. 60, no. 12, pp. 3705–3716, Dec. 2012.

[37] D. Tse and P. Viswanath, *Fundamentals of Wireless Communication*. Cambridge, U.K.: Cambridge Univ. Press, 2005.

[38] J. Poutanen *et al.*, "Significance of common scatterers in multi-link indoor radio wave propagation," in *Proc. IEEE Eur. Conf. Antennas Propag. (EuCAP)*, Apr. 2010, pp. 1–5.

[39] T. Komine and M. Nakagawa, "Fundamental analysis for visible-light communication system using LED lights," *IEEE Trans. Consum. Electron.*, vol. 50, no. 1, pp. 100–107, Feb. 2004.

[40] J. H. Y. Nah, R. Parthiban, and M. H. Jaward, "Visible light communications localization using TDOA-based coherent heterodyne detection," in *Proc. IEEE 4th Int. Conf. Photon. (ICP)*, Melaka, Malaysia, Oct. 2013, pp. 247–249.

[41] A. Al-Kinani, C.-X. Wang, H. Haas, and Y. Yang, "A geometry-based multiple bounce model for visible light communication channels," in *Proc. Int. Wireless Commun. Mobile Comput. Conf. (IWCMC)*, Sep. 2016, pp. 31–37.

[42] L. Feng, H. Yang, R. Q. Hu, and J. Wang, "mmWave and VLC-based indoor channel models in 5G wireless networks," *IEEE Wireless Commun.*, vol. 25, no. 5, pp. 70–77, Oct. 2018.

[43] B. Zhou, Q. Chen, P. Xiao, and L. Zhao, "On the spatial error propagation characteristics of cooperative localization in wireless networks," *IEEE Trans. Veh. Technol.*, vol. 66, no. 2, pp. 1647–1658, Feb. 2017.

[44] B. Zhou, Q. Chen, and P. Xiao, "The error propagation analysis of the received signal strength-based simultaneous localization and tracking in wireless sensor networks," *IEEE Trans. Inf. Theory*, vol. 63, no. 6, pp. 3983–4007, Jun. 2017.

[45] S. M. Kay, *Fundamentals of Statistical Signal Processing: Detection Theory*, vol. 2. Upper Saddle River, NJ, USA: Prentice-Hall, 1998.

[46] J. Kahn and J. Barry, "Wireless infrared communications," *Proc. IEEE*, vol. 85, no. 2, pp. 265–298, Feb. 1997.

[47] M. Yasir, S.-W. Ho, and B. N. Vellambi, "Indoor positioning system using visible light and accelerometer," *J. Lightw. Technol.*, vol. 32, no. 19, pp. 3306–3316, Oct. 1, 2014.